The Peptide Functionalized Inorganic Nanoparticles for Cancer-Related Bioanalytical and Biomedical Applications

Xiaotong Li [1,2], Minghong Jian [1,2], Yanhong Sun [1,2], Qunyan Zhu [1,*] and Zhenxin Wang [1,2,*]

1. State Key Laboratory of Electroanalytical Chemistry, Changchun Institute of Applied Chemistry, Chinese Academy of Sciences, Changchun 130022, China; lixiaotong@ciac.ac.cn (X.L.); mhjian@ciac.ac.cn (M.J.); yhyan@ciac.ac.cn (Y.S.)
2. School of Applied Chemistry and Engineering, University of Science and Technology of China, Hefei 230026, China
* Correspondence: zhuqy@ciac.ac.cn (Q.Z.); wangzx@ciac.ac.cn (Z.W.)

Abstract: In order to improve their bioapplications, inorganic nanoparticles (NPs) are usually functionalized with specific biomolecules. Peptides with short amino acid sequences have attracted great attention in the NP functionalization since they are easy to be synthesized on a large scale by the automatic synthesizer and can integrate various functionalities including specific biorecognition and therapeutic function into one sequence. Conjugation of peptides with NPs can generate novel theranostic/drug delivery nanosystems with active tumor targeting ability and efficient nanosensing platforms for sensitive detection of various analytes, such as heavy metallic ions and biomarkers. Massive studies demonstrate that applications of the peptide–NP bioconjugates can help to achieve the precise diagnosis and therapy of diseases. In particular, the peptide–NP bioconjugates show tremendous potential for development of effective anti-tumor nanomedicines. This review provides an overview of the effects of properties of peptide functionalized NPs on precise diagnostics and therapy of cancers through summarizing the recent publications on the applications of peptide–NP bioconjugates for biomarkers (antigens and enzymes) and carcinogens (e.g., heavy metallic ions) detection, drug delivery, and imaging-guided therapy. The current challenges and future prospects of the subject are also discussed.

Keywords: peptide ligand; inorganic nanoparticle; cancer; biosensing nanoplatform; nanomedicine

1. Introduction

Cancer is listed as the second foremost source of mortality worldwide in 2018 by the report of International Agency for Research on Cancer (IARC) of World Health Organization (WHO) [1]. Diagnostic and therapeutic agents play critical roles in the combat against this malignant disease. Because of their unique physicochemical properties such as large specific surface area, easy functionalization, and excellent optical, electrical, and magnetic properties, a variety of inorganic nanoparticles (NPs) have been extensively studied for early detection and treatment of cancers since 1996 [2–33]. For instance, due to their morphology (size, shape, and structure)-dependent localized surface plasmon resonance (LSPR), colloidal gold NPs (AuNPs) have been employed for the development of simple colorimetric sensing systems for sensitive detection of various cancer-related biomarkers and carcinogens [2–4,9–11,29]. Rare earth-doped up-conversion NPs (UCNPs), such as $NaYF_4$: Yb^{3+}, Er^{3+} UCNPs, can be excited by 808 nm and/or 980 near infrared (NIR) lasers, then emit at specific shorter wavelengths, resulting in improved detection specificity through a decrease of the bioluminesce background [6–8]. Because noble metal nanoclusters (size less than 2 nm in diameter), carbon dots (CDs, 1 to 10 nm in diameter), and semiconductor quantum dots (QDs) have a large Stokes shift and size-dependent excitation and emission spectra, they can be used as photomedicinal agents for in vitro/in vivo photoluminescence (PL) imaging [6,22,23]. Magnetic nanoparticles such as iron oxide NPs (IONPs) are excellent

theranostics for magnetic resonance imaging (MRI)-guided photothermal therapy (PTT) against cancer because they exhibit good biocompatibility, strong magnetic resonance (MR) contrast capacity, and high photothermal conversion efficiency [12–14]. In particular, the NPs prefer to accumulate in tumor sites by the size-dependent enhanced permeability and retention (EPR) mechanism [21,28,30–32]. This beneficial combination of physical and chemical properties has also given rise to an important application of NPs in the delivery of different anticancer drugs including traditional chemical drugs, small-interfering RNA (siRNA), and antigens [7,16,28,30,31].

Owing to their facile surface chemistry, the accumulation amounts of NPs in tumor site can be further increased through functionalization of NPs with various molecules, which normally enable to specifically recognize the tumor cells and/or tumor neovasculature by ligand-receptor interactions [5,6,9,10,12,13,17–20,33]. Among of these ligands, peptides with short amino acid sequences have attracted great attention because they have many important physiological functionalities and control nearly all vital functions in humans, including participation in signaling pathways as enzyme substrates, activation of immune defense as antigens, and effect on cellular membrane/organelle membrane functionality as drug carriers or lytic agents [10,12,14,17–20,33–36]. Especially, several peptides have been approved as drugs and an increasing number of peptides are entering clinical trials [35,36]. Therefore, a variety of peptide functionalized NPs have been synthesized and applied in bioanalytical and biomedical areas to perform targeting, diagnostic, and therapeutic functions in a single treatment procedure. For example, conjugation of NPs with peptides contained a cyclic RGD motif can generate novel nanosystems which exhibit high tumor-targeting ability through recognition of $\alpha_v\beta_3$ integrin receptor on tumor cell surface [37,38]. After being functionalized by cell penetrating peptides (CPPs), AuNP loading doxorubicin (DOX) led to improved survival time of mouse bearing a xenograft intracranial MDA-MB-231 breast tumor because the cellular internalization amount of DOX was increased significantly by the CPP modified AuNPs [39].

As an interactive nanobiotechnological scaffold, peptide functionalized NPs have thoroughly discussed in several reviews, which are categorized either by their components and/or their applications [10,12,14,17–20,33,34]. However, most of these reviews only described functionalization and application of a single type of NPs. For instance, the preparation and applications (biosensing, diagnosis, and therapy) of peptide modified AuNPs have been summarized in the reviews [10,17,20]. Spicer and colleagues provided a comprehensive overview of the peptide- and protein-functionalized nano-drug delivery vehicles, imaging species, and active therapeutics [14]. Desale and colleagues discussed the impact of CPPs in the field of nanotherapeutics [34]. For obtaining a broader view on the preparation and applications of peptide functionalized NPs, we strongly suggest that audiences read these excellent reviews. In this review, the discussion will focus primarily on the methods of preparing different peptide functionalized NPs and their applications in the cancer-related bioanalytical and biomedical areas including biosensing, bioimaging, drug delivery, and multimodal therapy (as shown in Figure 1). In particular, applications in the areas of cancer diagnosis and tumor-targeting drug delivery therapy are discussed in more detail through highlighted recent publications. Finally, we address future perspectives and the technical challenges of the peptide functionalized NPs as a promising theranostic of cancer.
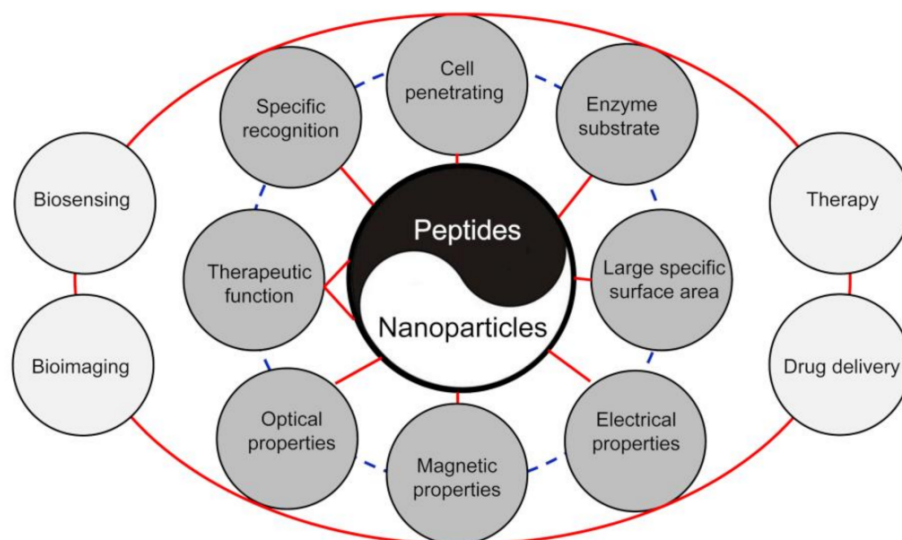
Figure 1. Schematic illustration of the effects of properties of peptide functionalized NPs on bioanalytical and biomedical areas including biosensing, bioimaging, drug delivery, and therapy. Combination of the biological properties of peptides and unique physicochemical properties of NPs can generate excellent nanosensing platforms with high sensitivity and specificity and nanotheranostics with high tumor-targeting capacity.

2. Synthesis of Peptide Functionalized Nanoparticles

Generally, the NPs were firstly produced by the hydrothermal or solvothermal approaches [40–64]. The as-prepared NPs were then modified with different peptides to achieve different functionalities for further applications. There are three main strategies for generating peptide functionalized NPs: (1) ligand exchange, (2) chemical conjugation, and (3) chemical reduction.

2.1. Ligand Exchange

The ligand exchange method is the simplest strategy for preparing peptide functionalized NPs, which essentially involves displacement of original ligand on NP surface by a specific peptide ligand and/or a mixture of peptide ligand [40,41]. Cysteine (Cys, C)-containing peptides have been used successfully to synthesize various peptide functionalized AuNPs by ligand exchange method because the thiol group (−HS) of cysteine can form strong S-Au covalent bond with surface Au atoms of AuNPs [40–52]. As early as 2004, Lévy and colleagues demonstrated that the pentapeptide, CALNN, can convert citrate-capped AuNPs into extremely stable, water-soluble AuNPs with some chemical properties analogous to those of proteins [42]. The CALNN modified AuNPs can be easily further functionalized with other biomolecules (e.g., biotin, DNA, etc.) for biological application. However, the Au−S covalent bond could be decomposed by the thiols (e.g., glutathione (GSH), Cys residues of proteins, etc.) in the living system. In order to eliminate the drawback, Tang and colleagues have developed an approach for synthesizing peptide functionalized AuNPs (peptide−Se−AuNPs) through the Au−Se bond instead of the Au−S bond by using peptide with Se modified cysteine [53–55]. The peptide−Se−AuNPs exhibit high colloidal stability, which can resist 5 mmol L^{-1} GSH and achieve a high-fidelity detection. Because phosphate has the ability to react with metallic cations such as Gd^{3+}, Fe^{3+}, and Zn^{2+} and forms robust metal−phosphate coordination bonds under mild conditions, peptides containing phosphorylated amino acid (e.g., phosphoseryl serine (Ser(P), S(P))) residue have been employed to transfer hydrophobic metallic NPs into aqueous phase and/or functionalize metallic NPs through the formation of metal–phosphate coordination bond [56,57]. For example, Liu and colleagues have developed a simple and robust route for surface functionalization of different NPs with the diameter less than 10 nm including $NaGdF_4$ nanodots, IONPs, zinc oxide NPs (ZnONP), AuNPs, and silver

NPs (AgNPs) by using tryptone as phase transfer agent [56]. The tryptone is a kind of peptide mixture which contains ca. 10–20% casein phosphopeptide with the sequence S(P)S(P)S(P)EE. The ligand exchange method is normally taken place under mild reaction condition, and can generate peptide functionalized NPs with high colloidal stability and diverse functionality.

2.2. Chemical Conjugation

Chemical conjugation a is two-step strategy to attach desired peptides on the NP surfaces. The NPs were firstly capped by stabilizers, such as derivatives of PEG (poly(ethylene glycol)) through ligand exchange and/or physical interactions (e.g., electrostatic interaction, hydrogen bonding, etc.), or hydrophilic shells (e.g., silica (SiO_2) and/or polydopamine (PDA) shell) through water-in-oil microemulsion method, which often have active groups that can be used to bind peptides [58–65]. The peptides were then conjugated on the NP surface through reaction with the stabilizers. The strategy is very useful to immobilized positively charged/neutral peptides on citrate-capped AuNPs, and transfer hydrophobic NPs into aqueous solution as well as peptide functionalization. In addition, the surface density of peptide on NPs can be adjusted by experimental parameters, such as reaction time and ratio of reagent in the reaction mixture, when the two-step strategy is employed to synthesize peptide functionalized NPs. Using EDC/sulfo-NHS (1-ethyl-3-(3-dimethylaminopropyl) carbodiimide hydrochloride/N-hydroxy sulfosuccinimide) coupling method, Bartczak and Kanaras successfully conjugated the positively charged peptide KPQPRPLS to carboxy-terminated oligoethyleneglycol stabilized AuNPs (OEG NPs, as shown in Figure 2) [58]. Recently, the monocyclic peptide (MCP, the CXC chemokine receptor 4 (CXCR4) antagonist) functionalized manganese-doped iron oxide NPs (MnIO NPs) were synthesized by Fu and colleagues [62]. Using the bifunctional ligand, DIB-PEG-NH$_2$ (3,4-dihydroxy benzyl amine-PEG-NH$_2$), as a phase transfer agent, the hydrophobic oleate-capped MnIO NPs were transferred into aqueous solution through formation of $Mn^{2+}/Fe^{3+}-DIB$ chelates. The MCP functionalized MnIO NPs were then synthesized through the amidation reaction between the amine group of PEG and carboxy group of peptide. Li and colleagues employed the carboxyl-terminated SiO_2 shell for transferring hydrophobic UCNPs from the organic phase to the aqueous phase, and conjugating peptide ligand with high tumor-targeting affinity [64].

2.3. Chemical Reduction

The peptide functionalized NPs can also be directly synthesized through the chemical reduction method [66–71]. The general operation steps of chemical reduction method are as follows: (1) pre-mixing the metal ion precursor and peptide in reaction solution, (2) adding a small quantity of reducing agent if required, (3) purifying as-prepared peptide functionalized NPs. The whole synthesis process is simple and normally carried out under mild aqueous conditions. In addition, the morphologies of NPs could be modulated by the change of reaction conditions, such as reaction time, pH value, peptide sequence, and ratio of metal ion precursor with peptide. In this strategy, the peptide is responsible for reduction of metal ions as well as stabilization of produced NPs [66–68]. Normally, the amino acid residues in peptides such as tyrosine (Tyr, Y), C, aldehyde-functionalized proline (Pro, P), and tryptophan (Trp, W) can reduce the metal ions to correspondent metals through electron transfer [66–68]. Si and Mandal reported an approach to prepare tripeptide functionalized AuNPs and AgNPs though an in situ reduction of HAuCl$_4$ or AgNO$_3$ by a W residue at the C-terminus of peptides (NH$_2$-L-Aib-W-OMe and tert-butyloxycarbonyl (Boc)-L-Aib-W-OH) at pH = 11 [66]. In addition, the peptide just plays the role of stabilizing agent, while other chemicals (e.g., such as sodium borohydride (NaBH$_4$) and ascorbic acid) are employed as the reducing agents [70,71]. In the presence of NaBH$_4$, Corra and colleagues found that the peptide H-H-dL-dD-NH$_2$ can be used as capping agent for the straightforward formation of PdNPs, PtNPs, and AuNPs with high monodispersity and colloidal stability in aqueous solution [71].
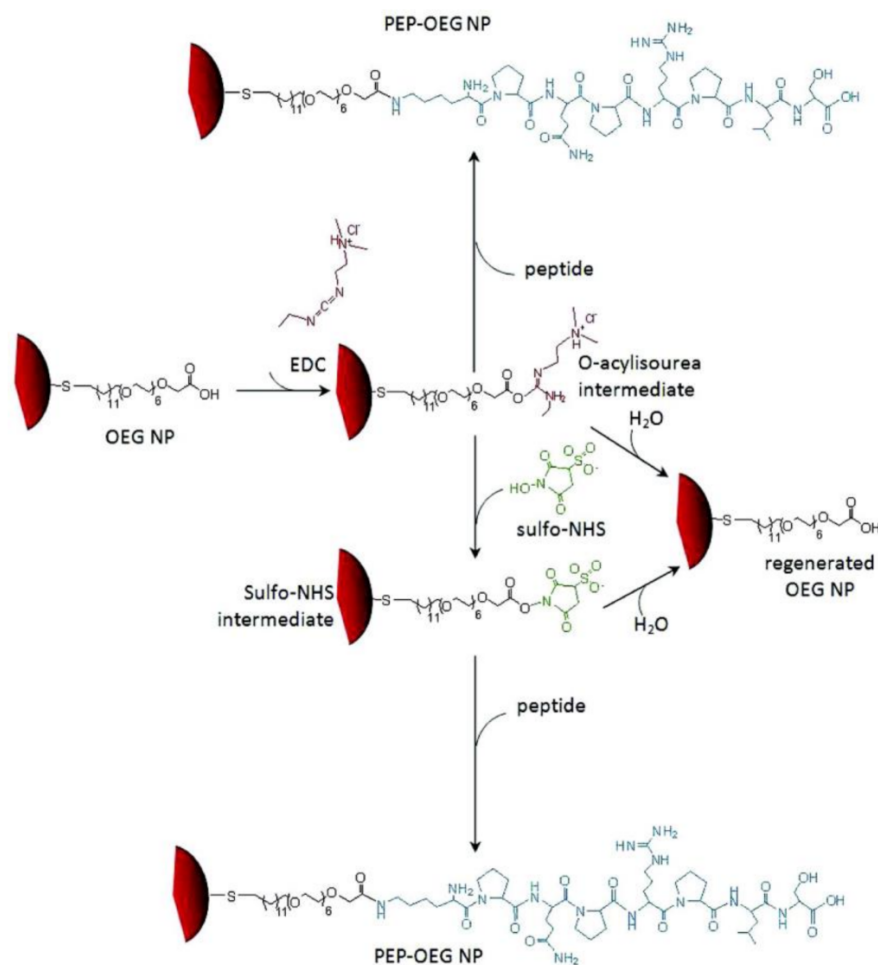
Figure 2. Schematic representation of amide bond formation between the KPQPRPLS peptide and OEG NPs by using EDC and Sulfo-NHS. The degree of peptide coupling as well as the colloidal stability of PEP-OEP NPs are strongly dependent on the experimental conditions (such as EDC and Sulfo-NHS concentrations, peptide concentration, reaction time, and reaction buffer) (Adapted from Bartczak and Kanaras 2011 [58], Copyright 2011 The American Chemical Society and reproduced with permission.).

3. Biosensing Platforms Based on Peptide Functionalized Nanoparticles

The peptide functionalized NPs have been extensively employed to construct biosensors/assays with various detection principles for detection of different analytes (some typical examples are included in Table 1) [72–131]. Among of these biosensors/assays, colorimetric assays and fluorescence sensing systems were well developed because of excellent optical properties of NPs.

Table 1. Peptide functionalized NP-based biosensors/assays with various detection principles for detection of different analytes. Normally, the peptide functionalized AuNPs were used to developed colorimetric assays, while peptide functionalized fluorescence NPs, such as UCNPs and QDs, were used to construct fluorescence sensing systems.

Nanoparticle	Peptide Sequence	Functionalization Strategy	Analyte	Detection Principle	Linear Range/ Detection Limit	Refs
AuNPs	NH_2-L-Aib-Y-OMe	Chemical reduction	Hg^{2+}	colorimetric assay	4 to 10 ppm/4 ppm	[72]
AuNPs	CALNN	Ligand exchange	Al^{3+}	colorimetric assay	0.5 to 6 mM/0.2 mM	[73]
AuNPs	CALNN/GSH	Ligand exchange	Pb^{2+}	colorimetric assay	500 nM to 15 mM/500 nM	[74]
AuNPs	GIRLRLEEIEYELKRISGGGC	Ligand exchange	Cu^{2+}	colorimetric assay	10 to 150 mM/1 mM	[75]
AuNPs	GSH	Ligand exchange	Pb^{2+}	colorimetric assay	30 nM to 2 mM/13 nM	[76]
AuNPs	RFPRGGDD	Ligand exchange	Ag+	colorimetric assay	10 nM to 1 mM/7.4 nM	[77]
AuNPs	EKEKEKPPPPC	Ligand exchange	Ni^{2+}	colorimetric assay	60 to 160 nM/34 nM	[79]
AuNPs	CALNNGK(Abscisic Acid)G	Ligand exchange	Abscisic acid glucose ester	colorimetric assay	5 nM to 10 mM/2.2 nM	[80]
AuNPs	WHSDMEWWYLLGGGGGC	Ligand exchange	Vascular endothelial growth factor receptor 1	colorimetric assay	0.2 to 10 nM/0.2 nM	[81]
AuNPs	KKHHHHHHKK	Ligand exchange	Prostate specific membrane antigen	colorimetric assay	2 to 10 nM/0.5 nM	[82]
AuNPs	Peptide-p53 and peptide-p14	Ligand exchange	Mdm2	colorimetric assay	30 to 50 nM/20 nM	[83]
AuNPs	H6GLRRAS(P)LG	Chemical conjugation	protein phosphatase 2A	colorimetric assay	-/-	[91]
AuNPs	GPDC or VP-ethylene diamine-DC	Ligand exchange	Dipeptidyl peptidase IV	colorimetric assay	0 to 12 U L^{-1}/1.2 U L^{-1} or 0 to 30 U L^{-1}/1.5 U L^{-1}	[94]
AuNPs	FGGFELLC	Ligand exchange	Aminopeptidase N	colorimetric assay	5 to 15 mg mL^{-1}/0.42 mg mL^{-1}	[95]
AuNPs	NAADLEKAIEALEKHLEAKGPC DAAQLEKQLEQAFEAFERAG	Ligand exchange	MMP-7	colorimetric assay	5 to 25 mg mL^{-1}/3.3 mg mL^{-1}	[98]
AuNPs	CCYKKKKQAGDV	Ligand exchange	Integrin GPIIb/IIIa	colorimetric assay	31.25 to 375 ng mL L^{-1}/31.25 ng mL L^{-1}	[99]
AuNCs	GSH	Chemical reduction	Cancer cell	colorimetric assay	-/-	[100]
AuNPs	FITC-KGRRPED(Ac)K-biotin and biotin-K(Cy5)HRHPRY(P)G	Ligand exchange	histone deacetylase and protein tyrosine phosphatase 1B	FRET	1 nM to 1 mM/28 pM and 0.015 to 0.3 nM/0.8 pM	[105]
UCNPs and carbon NPs	GHHYYGPLGVRGC	Chemical conjugation	MMP-2	FRET	10 to 500 pg mL^{-1}/10 pg mL^{-1}	[106]
UCNPs	(H)6YGKAGK-TAMRA	Ligand exchange	Trypsin	FRET	0.5−500 nM/0.05 nM	[108]
UCNPs and AuNPs	DDDDARC	Chemical conjugation and ligand exchange	Trypsin	FRET	12 to 208 ng mL^{-1}/4.15 ng mL^{-1}	[109]
UCNPs	CGRGGLEHDGGRK-Cy5	Chemical conjugation	Caspase-9	FRET	0.5–100 U mL^{-1}/0.068 U mL^{-1}	[114]
CdSe/ZnS QDs	Rhodamine-RGDC	Ligand exchange	Collagenase	FRET	0 to 5 mg mL^{-1}/-	[121]
Gold QDs	NES-linker-DEVD-linker-NLS	Chemical conjugation	Caspase-3	Fluorescence assay	-/-	[123]
Gold nanostars	LRRASLG	Chemical conjugation and ligand exchange	Protein kinase A	Surface-enhanced Raman spectroscopy	5 mU mL^{-1} to 5 kU mL^{-1}/5 mU mL^{-1}	[125]
AuNPs	3-mercaptopropionic acid-HSSKLQ-K (biotin)	Ligand exchange	Proteolytically active prostate specific antigen	Electrochemical sensor	0.1 to 100 ng mL^{-1}/27 pg mL^{-1}	[128]
AuNPs	RRRRRAGGPAC	Ligand exchange	Type IV collagenase	Quartz crystal microbalance biosensor	10 to 60 ng mL^{-1}/0.96 ng mL^{-1}	[131]

### 3.1. Colorimetric Assays Based on Peptide Functionalized AuNPs

The AuNP has been demonstrated as an excellent nanoprobe of colorimetric assays because its LSPR has an extremely sensitive response towards the dispersion state of AuNP [2–4,6,9–11]. The LSPR of AuNP displays a red shift along with a visual color change from red to blue, while the dispersion state of AuNP is changed from monodispersing state to aggregating state. Various colorimetric assays based on peptide functionalized AuNPs have been developed for detection of a wide range of cancer-related species such as metallic ions [72–79], small molecules [80], antigens/proteins [81–84], and enzymes [85–98].

Several colorimetric assays based on peptide functionalized AuNPs have been developed for detection of heavy metal ions since Si and colleagues employed the peptide (sequence, NH_2-L-Aib-Y-OMe) functionalized AuNPs-based colorimetric assay for sensing mercury ion (Hg^{2+}) at 2007 [72]. For instance, Yu and colleagues developed a GSH functionalized AuNPs (GSH-AuNPs) colorimetric assay for on-site detection of Pb^{2+} leaking from lead halide perovskite solar cells (PSCs) [76]. The Pb^{2+}-induced aggregation of GSH-AuNPs can read by both naked eye and UV–visible spectroscopy with detection limits (LODs) of 15 and 13 nmol L^{-1}, respectively. As shown in Figure 3, Parnsubsakul and colleagues reported a colorimetric assay based on zwitterionic polypeptide, EKEKEKPPPPC (($EK)_3$), capped 40 nm AuNP (termed as, AuNP-($EK)_3$) for sensing nickel ions (Ni^{2+}) [79]. By taking advantage of the alternate carboxylic (-COOH)/amine (-NH_2) groups, the zwitterionic peptide can function dually by being able to sense Ni^{2+} and maintain colloidal stability of AuNPs. Because the aggregation of AuNP-($EK)_3$ can be triggered by Ni^{2+} through interaction of the -NH_2 group of glutamic acid at the N-terminus of the peptide and Ni^{2+}, the color of AuNP-($EK)_3$ solution is changed from red to purple (as shown in Figure 3a). The AuNP-($EK)_3$-based colorimetric assay can detect Ni^{2+} as low as 34 nM within 15 min with a linear range of 60–160 nM (as shown in Figure 3b,c) with high selectivity (as shown in Figure 3d). In addition, AuNP-($EK)_3$-based colorimetric assay can be employed for detection of Ni^{2+} in soil, urine, and water samples since the internal -COOH/-NH_2 groups of glutamic acid and lysine confer stability to the AuNP-($EK)_3$.
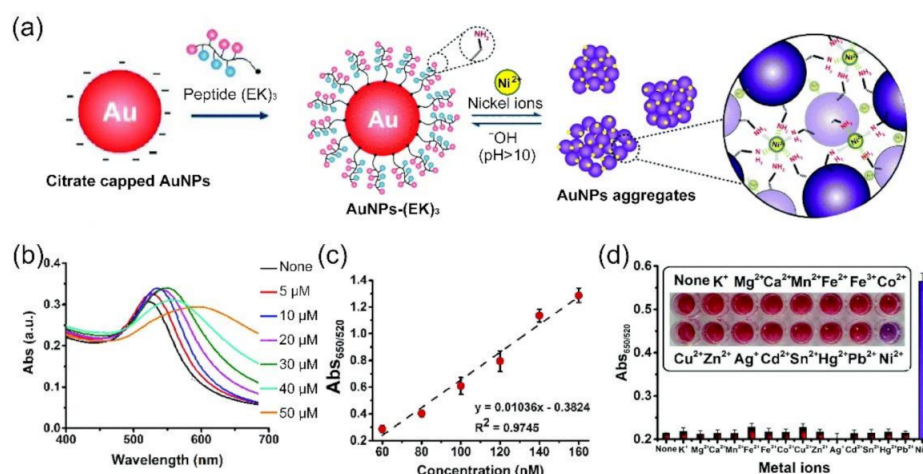
Figure 3. AuNP-($EK)_3$ nanoprobe-based colorimetric detection of Ni^{2+}. (**a**) Schematic illustration of AuNP-($EK)_3$ nanoprobe preparation and detection principle of Ni^{2+}, (**b**) UV–visible absorption spectra of AuNP-($EK)_3$ at different concentrations of Ni^{2+} (0–50 μM), (**c**) linear calibration plot of AuNP-($EK)_3$ versus Ni^{2+} concentrations in the range of 60–160 nM, (**d**) selectivity of AuNP-($EK)_3$ toward different metal ion species. The zwitterionic region of the ($EK)_3$-peptide can bind to Ni^{2+} due to the presence of an -NH_2 or -COOH group and the unfilled d-orbital of Ni^{2+}, leading to the aggregation of AuNPs. As a result, in the presence of Ni^{2+}, the color of the AuNP-($EK)_3$ solution is changed from red to purple. (Adapted from Parnsubsakul et al. 2018 [79], Copyright 2018 The Royal Society of Chemistry and reproduced with permission.).

It is found that abnormal enzyme activity is closely related to tumorigenesis and development, making enzymes such as kinases, proteases, and peptidases as important biomarkers for early cancer diagnosis and targets for therapeutic drug development. The colorimetric assays based on peptide functionalized AuNPs can be employed to determine enzyme activity and act as a screening inhibitor of the enzyme, when the AuNPs are functionalized by peptide substrate of enzyme [85–98]. As early as 2006, Wang and colleagues demonstrated that the interactions of biotinylated peptide substrate functionalized AuNPs and avidin-modified AuNPs could be employed to develop a colorimetric assay for the evaluation of kinase activity and inhibition [85]. In this case, using γ-biotin-ATP as a cosubstrate, the kinase reaction results in the biotinylation of the peptide substrate on AuNPs. Mao and colleagues proposed a one-pot and one-step colorimetric sensing method for detecting activity of aminopeptidase N (APN) based on a peptide (NH_2-FGGFELLC-Ac) functionalized AuNPs/cucurbit[8]uril (pep-AuNPs/CB[8]) supramolecular structure which was formed by the crosslinking of pep-AuNPs with CB[8] [95]. In the presence of APN, the pep-AuNPs/CB[8] supramolecular structure is disassembled because the peptide will be hydrolyzed by APN. The activity of APN can be determined through the absorbance changes based on the assembly/disassembly of AuNPs. Under optimized conditions, the as-proposed colorimetric assay has a linear range from 5 μg/mL to 15 μg/mL with a LOD of 0.42 μg/mL, which can be used to detect APN in serum samples. As shown in Figure 4a,b, Goyal and colleagues reported a heterogeneous protease assay on polyvinylidene fluoride (PVDF) membrane based on aggregation of peptide-functionalized AuNPs [98]. Using the matrix metalloproteinase-7 (MMP-7) substrate (AIEALEKHLEAKGPCDAAQLEKQLE-QAFEAFERAG) functionalized AuNPs as typical example, the proteolysis-driven aggregation of AuNPs on the membrane yields a colorimetric response from reddish/brownish to violet with increasing concentration of MMP-7 (as shown in Figure 4c). The color change can be distinguished by the naked eye for MMP-7 concentrations above 165 nM (visual LOD), which is ~4 times lower than that of the same assay performed in homogeneous solution. The practicability of as-proposed assay was demonstrated by detection of MMP-7 in synthetic urine. The colorimetric based on the proteolysis-driven aggregation of AuNPs on PVDF membrane could be used to detect other proteases by using AuNPs functionalized with specific peptides. The proposed approach would be ideal for applications in resource-limited settings.
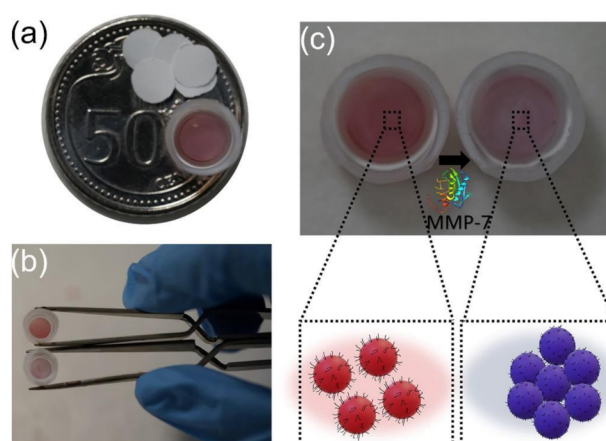
Figure 4. (**a**) Comparison of the size of the membrane with respect to a 50 cents coin, and (**b**) photograph and (**c**) schematics of the assay with peptide functionalized AuNPs on PVDF membrane, which yields a change in color from reddish to violet, due to aggregation induced by MMP-7. The MMP-7 peptide substrate functionalized AuNPs were deposited on PVDF membrane. The AuNPs aggregate on PVDF membrane because of increased electrostatic interparticle attraction upon proteolysis by MMP-7. (Adapted from Goyal et al. 2020 [98], Copyright 2019 Elsevier B.V. and reproduced with permission.).

In addition, peptide-functionalized AuNPs can be used as artificial enzymes (nanozymes) for developed colorimetric assays [99,100]. Feng and colleagues established a colorimetric assay for detection of cellular GSH level by the inhibition effect of GSH on the peroxidase-like activity of GSH stabilized AuNCs (GSH-AuNC) [100]. Because the GSH-AuNC catalytic oxidation of peroxidase substrate 3,30,5,50-tetramethylbenzidine (TMB) is effectively inhibited by GSH, the absorbance at 652 nm is linearly decreased by increasing GSH concentration within a range from 2 to 25 mM. The as-proposed assay provides a powerful tool for identifying cancer cells since the overall GSH level in cancer cells is much higher than that in normal cells.

3.2. Fluorescence Assays Based on Peptide Functionalized NPs

Due to the overlap of maximum fluorescence emission of fluorescent probes with UV–visible absorption spectrum (LSPR band) of AuNPs, there is extreme possibility for development of "turn-on" fluorescence assay by peptide functionalized AuNPs [55,101–105]. Recently, Zhang and colleagues developed a "turn-on" fluorescence assay-based peptide functionalized AuNPs nanosensor for simultaneous detection of multiple posttranslational modification (PTM) enzymes, such as histone deacetylase (HDAC) and protein tyrosine phosphatase 1B (PTP1B) [105]. The AuNPs were functionalized by two biotinylated peptide substrates including (FITC-KGRRPED(Ac)K-biotin) with Lys(Ac) as the acetylation site and (biotin-K(Cy5)HRHPRY(P)G) with Y(P) as the phosphorylation site. The AuNPs exhibit strongly quenching capability on the fluorescence of FITC and Cy5. In the presence of specific enzyme pairs (HDAC/rLys-C endoproteinase and PTP1B/Cytochrome oxidase), FITC and Cy5 fluorescence are gradually recovered during enzymatic digestion of peptides, respectively. The activities of HDAC and PTP1B can be quantitatively determined by the recovery of FITC and Cy5 fluorescence, respectively. The approach has LODs of 28 pM for HDAC and 0.8 pM for PTP1B, and can be further employed for screening inhibitors of PTM enzymes and detecting activities of PTM enzymes in HeLa cells.

With the multiple advantages including robust and high photostability, low toxicity, and deep tissue penetration with minimal autofluorescence background, UCNPs are rapidly emerging as strong contenders for the traditional down conversion-based fluorescence NPs/fluorescence dyes in biosensor construction because UCNPs are able to convert near-infrared (NIR) light into higher-energy and multicolor UV–visible emission light [6–8]. Recently, peptide-functionalized UCNP-based fluorescence resonance energy transfer (FRET) systems have been also used to detect various enzymes [106–114]. UCNPs are normally synthesized in organic phase for obtaining high fluorescence quantum yield and low nanocrystal defect. Therefore, the UCNPs should be firstly transferred into aqueous medium by coating a hydrophilic layer, such as SiO_2 and PDA, and then conjugated by peptides. In 2015, Zeng and colleagues reported a facile method for preparation of highly compact and stable biofunctionalized UCNPs through peptide-mediated phase transfer strategy [108]. The peptide-functionalized UCNP can be used for high-sensitive detection of trypsin and in vivo evaluation of apoptosis for chemotherapy efficacy of cancer by the FRET between TAMRA (acceptor) and green UCL of UCNP (donor). Recently, Liu and colleagues have developed a series of peptide functionalized UCNP-based FRET sensing platforms for detecting activities of caspases and evaluating treatment efficiency of anticancer drugs (e.g., cisplatin) [65,113,114]. As shown in Figure 5, they constructed a FRET sensing platform for detection of caspase-9 activity in vitro and in vivo by using UCNP@SiO$_2$ core@shell NPs functionalized with a Cy5 labeled peptide containing specific motif LEHD for caspase-9 cleavage [114]. In this case, the red up-conversion luminescence (UCL) emission of UCNP@SiO$_2$ is efficiently quenched by Cy5. In the presence of caspase-9, the Cy5 dissociated from UCNP@SiO$_2$ surface by enzymatic cleavage of LEHD, resulting in recovery of red UCL emission of UCNP@SiO$_2$. It is found that the intracellular caspase-9 activity level of cisplatin-treated MG-63 cells is higher than that of cisplatin-treated SW480, indicating that MG-63 cell is sensitive to the cisplatin treatment.
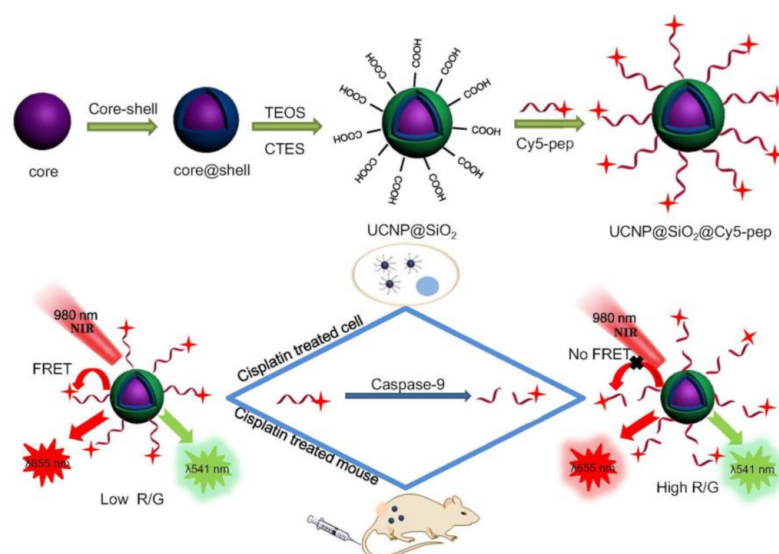
Figure 5. The schematic representation of UCNP-based FRET sensing platform for the detection of caspase-9 activity both in vitro and in vivo by using UCNPs as the energy donor and Cy5 as the energy acceptor. The Cy5 labelled peptide with specific motif LEHD for caspase-9 cleavage were conjugated with carboxyl modified UCNP@SiO$_2$ through covalent attachment. (Adapted from Liu et al. 2019 [114], Copyright 2019 Elsevier B.V. and reproduced with permission.).

The peptide-based photoluminescent QDs/metal clusters-based fluorescence sensing systems have also been developed for sensitive and selective detection of enzymes such as proteases because these nanoprobes have unique optical properties including high quantum yields, excellent optical stability, narrow fluorescence FWHM and tunable maximum emission wavelength [115–120]. Most of these FRET sensors consist of a QDs/metal cluster donor conjugated with a short-sequence peptide substrate carrying the acceptor (e.g., fluorescent dye). In order to increase the FRET efficiency, several acceptor peptides can be conjugated to the same QD. As early as 2006, Shi employed a rhodamine labeled tetrapeptide RGDC to replace the hydrophobic trioctylphosphine oxide (TOPO) ligand of CdSe/ZnS QD [121]. The rhodamine labeled RGDC functionalized CdSe/ZnS QD was successfully used as sensing platform for sensitive detection of MMP activity through the FRET between rhodamine (acceptor) and CdSe/ZnS QD (donor). Lin and colleagues reported subnanometer photoluminescent gold QDs (GQDs) with a peptide ligand that contains nuclear export signal (NES) sequence, nuclear localization signal (NLS) sequence, and capsase-3 recognition sequence (DEVD), which could be used as molecular probes for the real-time monitoring of cellular apoptosis [123].

4. Employing Peptide Functionalized Nanoparticle as Positive Tumor-Targeting Nanomedicines

Over recent years, the research community is acknowledging that the peptides can be used as important ligand/building blocks for designing positive tumor-targeting nanomedicines because of their advantages, including their relatively small size, biocompatibility, easy chemical synthesis and modification, and various biofunctionalities [35,36,132]. In particular, (1) large scale synthesis of peptides can be easily achieved by solid-phase synthesis technology, which presents a convenient and economical option for biomedical applications; (2) peptides have good biocompatibility; (3) many peptides have sequence-dependent bioactivity/functions, such as specifically binding to receptors/antigens on (sub)cellular membranes, high cellular permeability, tumor microenvironmental responsiveness, triggering immune response, etc.; (4) the terminus or side chains of peptides provide plenty reactive groups (i.e., amino (-NH$_2$) and carboxyl (-COOH) groups) for conjugating others functional molecules, such as drugs or carriers with peptides. With the rapid development of nanotechnology, the peptide-functionalized NPs have been ex-

tensively used as nanoprobes and/or nanocarriers for precision oncology [34,38,39,133]. Normally, tumor-specific targeting peptides are used to prepare positive tumor-targeting nanomedicines, which are mainly identified via bio-inspired techniques (biomimetic peptides) or large-scale screening of peptide libraries (such as phage display peptide libraries and chemical peptide libraries) [134,135]. For instance, Wang and colleagues successfully screened two peptide ligands form a one-bead one compound (OBOC) peptide library for the tumor biomarker human epidermal growth factor receptor 2 (HER2) by using in situ single bead sequencing on a microarray [136].

4.1. Enhancing Cellular Internalization and Targeting Cancer Cells

Some peptides, known as CPPs, can be uptaken specifically by certain cell organelles through multiple interactions with the exposed plasma membrane [34]. Several CPPs have been identified since the first CPP (peptide with 86 amino acids derived from HIV transactivator of transcription (TAT)) was discovered in 1980 [137]. Generally, CPPs are short-chain amino acid residues (5–30 residues), which are classified into three categories, cationic CPPs, amphipathic CPPs, and hydrophobic CPPs. Cationic CPPs and amphipathic CPPs are normally used to enhance cellular internalization of NPs. After conjugation with CPPs, the cellular internalization of NPs can be enhanced significantly. In particular, the peptides containing special lysine (K)-, arginine (R)-, or proline (P)-rich motifs (known as nuclear localization sequences (NLSs)) can efficiently transport NPs into the nucleus [133,138–149]. As early as 1999, Josephson and colleagues found that Tat peptide modified SPIOs were internalized into lymphocytes over 100-fold more efficiently than nonmodified NPs [138]. De la Fuente and Berry found that the Tat-derived CPP (GRKKRRQRRR) functionalized AuNPs exhibited high cell membrane permeability, and were able to target the cell nucleus [141]. In 2008, Sun and colleagues reported that $CALNNR_8$/CALNN co-functionalized AuNPs could target different intracellular components through adjusting the ratio of the $CALNNR_8$ to CALNN [143]. After incubation with HeLa cells, the peptide mixture ($CALNNR_8$:CALNN = 1:9) functionalized AuNPs had translocated into the cell nucleus, while $CALNNR_8$ functionalized AuNPs remained in the cytoplasm. Recently, Wang and colleagues demonstrated that Tat (Ac-YGRKKRRQRRR) functionalized cosolvent-bare hydrophobic QD (cS-bQDs-Tat) exhibited extraordinary intracellular targeting performance with the nucleus as the model target [133].

Because RGD motif can bind to integrins with high specificity and affinity and integrin $\alpha_v\beta_3$ is highly overexpressed in many types of cancer cells, the RGD peptide family have been employed as peptide ligand resources for preparation of peptide-functionalized NPs with positive tumor-targeting capacity [150–164]. Among the RGD peptide family, the tumor-targeting abilities of cyclic RGD peptides (such as c(RGDfV) are better than those of linear RGD peptides. As early as 2008, Shukla and colleagues prepared the fluorescein isothiocyanate (FI) and cRGDyK peptide functionalized G5 poly(amidoamine) (PAMAM) dendrimer-entrapped 3 nm AuNPs, which exhibited strong tumor microvasculature targeting efficacy [150]. As shown in Figure 6, Yan and colleagues reported a RGD functionalized ultra-small $Gd(OF)_3$: Ce, Tb nanocrystals (about 5 nm in diameter) for simultaneously targeted imaging cell cytoplasm and nucleus [154]. The as-prepared RGD@ $Gd(OF)_3$: Ce, Tb nanocrystals were successfully used as fluorescence label for imaging simultaneously the cytoplasm and nucleus of living cells including cancer cells and stem cells since they exhibit good water dispersibility, excellent cellular biocompatibility and targeted ability, high photostability, and double emissions (545 nm and 587 nm) with high quantum yield. After RGD@ $Gd(OF)_3$: Ce, Tb nanocrystal labeling, the living cells exhibited very high signal-to-noise ratio of fluorescence emissions. Therefore, RGD@ $Gd(OF)_3$: Ce, Tb nanocrystals show great promise for cellular and molecular-level bioimaging applications. Tang and colleagues have successfully conjugated cRGDfK ((Arg-Gly-Asp-DPhe-Lys) on Ag_2S QDs [155]. The cRGDfK modified Ag_2S QDs can be selectively internalized by tumor cells and accumulated in tumor tissue, respectively. In particular, the cRGDfK-Ag_2S QDs exhibit an exceptionally high tumor-to-liver uptake ratio and efficient renal excretion

ability, demonstrating it as excellent nanoprobe for molecular imaging of diseases and the monitoring of treatment response.
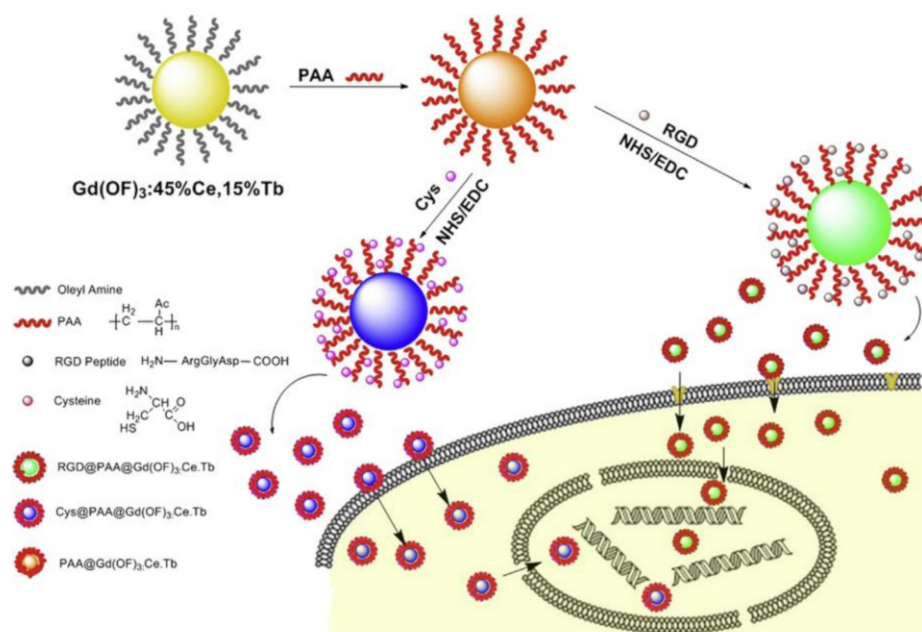
Figure 6. Schematic illustration for the synthesis of RGD and Cys functionalized Gd(OF)$_3$: Ce, Tb nanocrystals and their targeted imaging. The oleylamine capped nanocrystals were modified by polyacrylic acid (PAA) to form the PAA capped Gd(OF)$_3$: 45%Ce, 15%Tb nanocrystals (PAA@Gd(OF)$_3$: 45%Ce, 15%Tb) through a ligand exchange method. RGD peptide and cysteine were conjugated to the nanocrystals surface by EDC/NHS chemistry (Adapted from Yan et al. 2015 [154], Copyright 2015 Elsevier Ltd. and reproduced with permission.).

Other peptide ligands, such as the peptides containing PSP/SP motif, anti-Flt1 peptide (CGNQWFI, AF), and Nestin peptides (AQYLNPS, Nes) have also been used to prepare peptide-functionalized NPs with positive tumor-targeting capacity [57,62,64,165–172]. Because they show highly specific recognition of tumor neovasculature compared to normal blood vessels [173], Chen and colleagues prepared a retro-inverso SP peptide (_D_(PRPSPKMGV(p-S)VS), where p-S is a phosphoseryl serine residue, and others are retro-inverso amino acids) and a cytosol-localizing internalization peptide (KVRVRVRV(dP)P(p-T)RVRERVK, where p-T is a phosphoseryl threonine residue, and dP is Dproline) co-modified NaGdF$_4$ ND, which shows high tumor-targeting ability, and facilitates renal clearance [57]. The as-prepared peptide functionalized NaGdF$_4$ NDs were successfully used as high efficient contrast agent of MRI for in vivo imaging small drug induced orthotopic colorectal tumor (ca., 195 mm^3 in volume) in mice. Li and colleagues prepared two SP peptides (L-SP5-C peptide (sequence: _L_(CSVSVGMK(Ac)PSPRP-NH$_2$) and L-SP5-H peptide (sequence: _L_(HSVSVGMK(Ac)PSPRP-NH$_2$)) modified NaErF$_4$:Yb@NaGdF$_4$:Yb core@shell UCNPs (UCNP@SiO$_2$-L-SP5-C and UCNP@SiO$_2$-L-SP5-H) [64]. Due to the tumor-targeting affinity of PSP motif in the peptide ligands, both UCNP@SiO$_2$-L-SP5-H and UCNP@SiO$_2$-L-SP5-C can be employed as positive tumor targeting contrast agents for UCL/T$_1$-weighted MR dual-mode imaging. They found that UCNP@SiO$_2$-L-SP5-C has relatively high affinity with HCT116 colorectal cancer (CRC) subtype.

4.2. Cancer Therapy

4.2.1. Antiangiogenic Therapy

It is demonstrated the tumor growth and metastasis can be suppressed significantly through disrupting the tumor vascularization [174–176]. The tumor inhibition abilities antiangiogenic agents can be reinforced when they are loaded on the NPs. Several peptide-

functionalized NPs with antiangiogenic properties have been employed for directly inhibiting pathological angiogenesis [177–181]. Very recently, Li and colleagues synthesized an anti-Flt1 peptide (AF, CGNQWFI) functionalized AuNC (ca. 2 nm in diameter) with targeted antiangiogenic property (as shown in Figure 7) [181]. The AF@AuNCs exhibit effectiveness in inhibiting both tube formation and migration of the endothelial cells in vitro since the interaction between vascular endothelial growth factor receptor 1 (VEGFR1) and its ligands could be blocked by AF and the expression of VEGFR2 could be downregulated (as shown in Figure 7a). The in vivo chick embryo chorioallantoic membrane (CAM) experiment and antitumor experiment with a mouse-bearing CAL-27 tumor verify that the antiangiogenesis and tumor inhibition effect of AF@AuNCs is much stronger than that of free AF (as shown in Figure 7b,c).
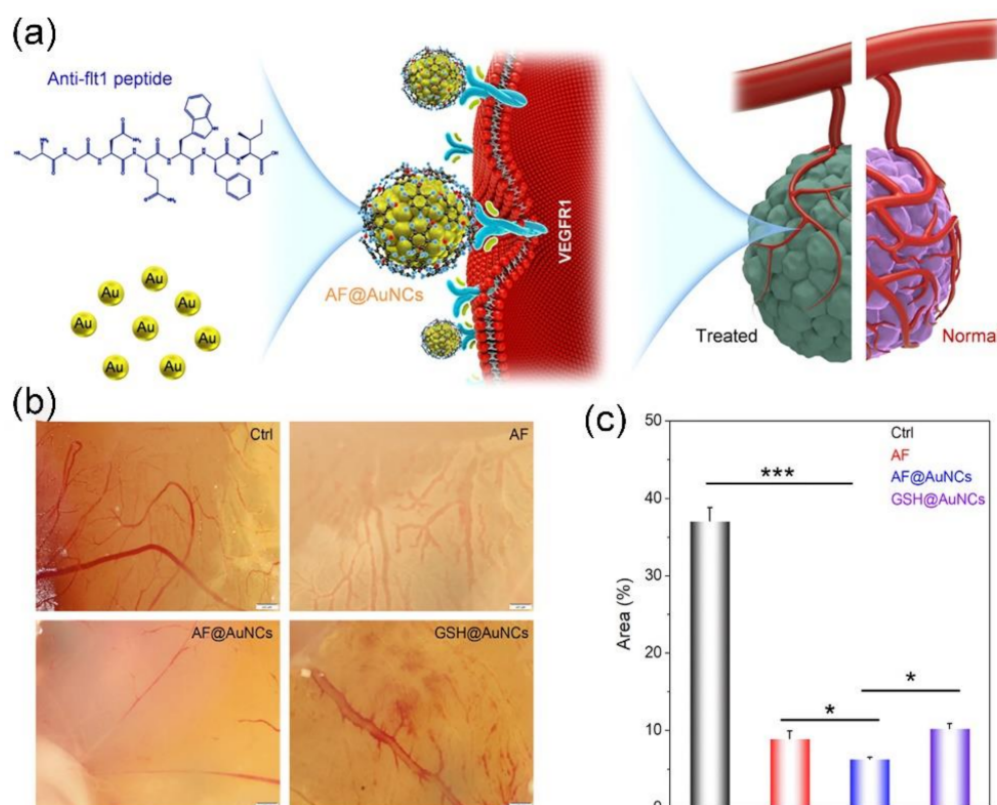
Figure 7. Antiangiogenic cancer therapy by AF@AuNCs. (**a**) Schematic illumination of Anti-Flt1 peptide templated AF@AuNCs for antitumor angiogenesis, (**b**) inhibition of CAM angiogenesis after incubation with AF, AF@AuNCs, and GSH@AuNCs at a concentration of 100 μg/mL and the incubation time was 48 h, and (**c**) comparison of the number of vessels in the AF, AF@AuNCs, and GSH@AuNCs after incubation for 48 h at a concentration of 100 μg/mL in the CAM model. AF@AuNCs were prepared by mixing AF with HAuCl$_4$. The AF@AuNCs show enhanced ability in inhibiting angiogenesis in fertilized eggs than those of pure AF and GSH@AuNCs. Data represent means $\pm$ SD ($n = 3$). * $p < 0.05$ and *** $p < 0.001$, data with significant difference (Adapted from Li et al. 2021 [181], Copyright 2021 American Chemical Society and reproduced with permission.).

4.2.2. Photothermal Therapy

NP-based PTT has been demonstrated as a promising technology for eliminating tumors because photothermal conversion NPs have the ability to efficiently convert light energy into heat [9,10,14,17,182–184]. According to current mainstream cancer treatments, an ideal PTT nanoplatform should have following three features: (1) strong tumor-targeting capability for initial delivery to the required site, (2) ability to efficiently convert NIR light energy into heat for improving tissue penetration, (3) high contrast capability for facilitat-

ing imaging-guided therapy by MRI, Computed Tomography (CT), and/or fluorescence. Peptide functionalized NPs can satisfy these features because the NPs have unique photothermogenic and optical properties and passive tumor-targeting ability through EPR effect, and peptide ligand have positive tumor-targeting ability [62,185–195]. In particular, the peptide-functionalized NPs could be used as nanomedicines for achieving synergistic photothermal therapy and immunotherapy because some peptides have been demonstrated as therapeutic agents which can efficiently kill cancer cells and inhibit tumor growth [62]. Li and colleagues constructed cancer cell nuclear-targeted copper sulfide NPs (CuS@MSN-TAT-RGD NPs) with a significant photothermal effect to completely kill residual cancer cells and prevent local cancer recurrence through the surface modification of RGD and TAT peptides on 40 nm porous silica coated copper sulfide NPs (CuS@MSN NPs) [189]. The CuS@MSN-TAT-RGD NPs exhibited an outstanding targeting effect toward the cancer cells because of the interaction of RGD with $\alpha_v\beta_3$, and further transport to nucleus due to the surface decoration of TAT peptides. Under the irradiation of 980 nm NIR laser, the CuS@MSN-TAT-RGD NPs rapidly increase the temperature of the nucleus and induce an exhaustive apoptosis of the cancer cells through destroying the genetic substances. Using mouse-bearing HeLa tumor as a model, the in vivo experiments demonstrated that the xenografted HeLa tumor was completely removed after 2 weeks with one PTT treatment of CuS@MSN-TAT-RGD NPs, and there was no recurrence of the cancer. Fu and colleagues constructed a multifunctional NP (MnIOMCP) for positive tumor-targeting T_1-weighted and T_2-weighted (T_1-T_2) dual-modal MRI-guided bio-PTT through bioconjugation of the CXCR4 antagonist monocyclic peptides (MCP) with MnIO NPs [62]. The MnIOMCP shows both T_1-weighted and T_2-weighted MR contrast abilities, reasonable photothermal conversion efficiency under 808 nm NIR laser irradiation, and the strong tumor-targeting and inhibition of cancer cell growth by the interactions of MCP with overexpressed CXCR4 in the tumor. The experimental result of in vivo experiment demonstrates that MnIOMCP can accumulate in MCF-7 tumors as high as $\sim15.9\%$ ID g^{-1} at 1 h after intravenous injection into mice with the aid of an external magnetic field (MF), creating the opportunity for complete eradication of the tumor by T_1-T_2 dual-modal MRI-guided bio-PTT. The peptide functionalized NPs can be used as theranostic for achieving PTT and optical bioimaging simultaneously under single laser irradiation. For instance, Huang and colleagues synthesized a tumor-homing peptide, LyP-1(CGNKRTRGC) and NIR dye IR780 co-functionalized gold nanoprisms (GNPs/IR780-LyP-1) [193]. Under 660 nm laser irradiation, the as-obtained GNPs/IR780-LyP-1exhibited the strong surface-enhanced resonant Raman scattering (SERS) property and photothermal conversion efficiency, which can serve as an excellent theranostic for SERS imaging-guided PTT of tumor.

4.2.3. Radiotherapy

The peptide functionalized NPs are also being used as positive tumor-targeting radiation dose enhancer in cancer radiotherapy [173,196–200]. Cruje and colleagues found that the RGD peptide (CKKKKKKGGRGDMFG) functionalized AuNPs exhibited higher enhancement of radiotherapy than that of PEGylated AuNPs [196]. In addition, the smaller RGD peptide functionalized AuNPs (14 nm in diameter) have a three-fold therapeutic enhancement as compared to larger RGD peptide functionalized AuNPs (50 nm in diameter) in MDA-MB-231 cells at clinically relevant 6 MV energy. Recently, Hafsi and colleagues explored the possibility of enhancing two modalities of radiotherapy, X-rays and protons, using RGD peptide functionalized magnetosomes (magnetosomes@RGD) [200]. Here, the magnetosomes are bacterial biogenic magnetic NPs naturally coated with a biological membrane. Compared to unmodified magnetosomes, magnetosomes@RGD exhibited remarkably high cellular internalization as well as efficacy of radiotherapy both in vitro and in vivo. The experimental results indicate that the magnetosomes@RGD can be used as tumor radioenhancers for both X-rays and protons. Interestingly, combined to magnetosomes@RGD, proton therapy showed higher killing efficacy than that of X-ray therapy at equivalent dose.

4.2.4. As Tumor Microenvironment Responsive Nanoprobes with Precision Tumor-Targeting

Owing to their high specificity and sensitivity, several peptide functionalized NP-based nanocomposites have been employed as tumor microenvironment responsive theranostics for precision diagnosis and/or imaging-guided therapy of tumors [201–207]. For instance, Zhao and colleagues constructed the MMPs/pH dual-stimuli-responsive and reversibly activatable nanoprobe for precision tumor-targeting and fluorescence imaging-guided photothermal therapy through asymmetric cyanine and glycosyl functionalized gold nanorods (AuNRs) with MMPs-specific peptide [203]. As shown in Figure 8, Han and colleagues prepared gemcitabine (GEM) derivative (GEM-GFLG-NH$_2$) and pH (low) insertion peptide (pHLIP, AEQNPIYWARYADWLFTTPLLLLDLALLVDADEGT) cofunctionalized magnetic NPs (denoted as GEM-MNP-pHLIP) for targeted therapy of pancreatic cancer with GEM [205]. The pHLIP largely increased the binding affinity of the GEM-MNP-pHLIP to PANC-1 cells. The targeted delivery and effective accumulation of GEM-MNP-pHLIP in vivo were confirmed by MRI enhanced by the underlying magnetic NPs (i.e., Fe$_3$O$_4$ NPs). After disruption of the dense stroma by metformin (MET), the GEM-MNP-pHLIP treatment exhibited a remarkably improved therapeutic efficacy (up to 91.2% growth inhibition ratio over 30 d of treatment) of both PANC-1 subcutaneous and orthotopic tumor mice models. Very recently, Zha and colleagues synthesized dual-Epstein-Barr virus (EBV)-oncoproteins targeting and pH-responsive NaGdF$_4$: Yb^{3+}, Er^{3+}@NaGdF$_4$ UCNPs (termed as (UCNP-Pn, n = 5, 6, and 7) for precision targeting, monitoring, and inhibition of EBV-associated cancer through conjugation of dual-EBNA1 (a latent cellular protein)/LMP1 (a transmembrane protein)-targeting peptide on UCNP [206]. Because of their transmembrane LMP1 targeting ability and the pH responsiveness capacity, the UCNP-Pn exhibits high cellular internalization in EBV-infected cells, strong UCL signal enhancement upon targeted dual-protein binding, efficacious EBV cancer inhibition in vitro and in vivo.
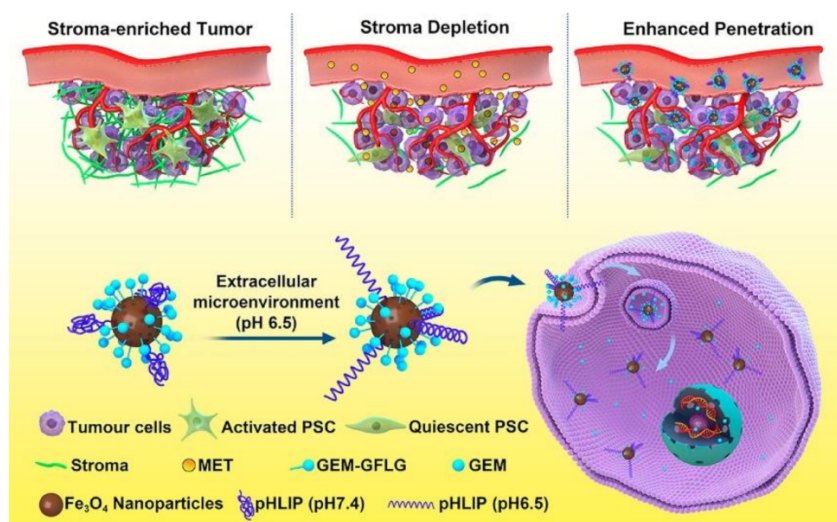
Figure 8. Schematic representation of MET-induced stromal depletion for enhancing the penetration and cathepsin B-triggered release of GEM carried by Fe$_3$O$_4$ NPs in the lysosome of pancreatic ductal adenocarcinoma (PADC) cells. The pHLIP facilitates the internalization of the underlying Fe$_3$O$_4$ NPs by inserting into cell membranes because it can format stable transmembrane α-helix in acidic tumor microenvironment. Once internalized into the cancer cells, GEM will be released in lysosome upon cleavage of its linker (i.e., GFLG peptide) by cathepsin B. In the animal experiments, MET was intraperitoneally injected to deplete the dense stromal barrier of PDAC prior to the injection of the above nanoagents to facilitate the effective delivery of GEM. (Adapted from Han et al. 2020 [205], Copyright 2020 American Chemical Society and reproduced with permission.).

4.2.5. Employing Peptide Functionalized NPs as Positive Tumor-Targeting Drug Carries

The peptide functionalized NPs have been extensively employed to avoid non-specific delivery-related issues in the diagnosis and therapy of cancer. Especially, the role of CPP functionalized NPs has been explored in the areas, such as molecular imaging and anticancer drug delivery, because CPPs aid in cellular internalization of various NPs without damaging the cell, and the CPP functionalized NPs can be served as cargos for intracellular transport of various species including radioactive isotopes [173,208–210], small molecules [208,211–231], oligonucleotides [232–256], and other peptides [63,257].

As early as 2011, Yang and colleagues prepared a multifunctional nanotheranostic based on superparamagnetic iron oxide NPs (SPIOs) for targeted drug delivery and positron emission tomography/MRI (PET/MRI) dual-modality imaging of tumor [208]. The anticancer drug, DOX was loaded onto the PEGylated SPIO nanocarriers via pH-sensitive bonds, and the tumor targeting peptides c(RGDfC and ^{64}Cu chelators, macrocyclic 1,4,7-triazacyclononane-N, N$'$, N$''$-triacetic acid (NOTA), were conjugated onto the distal ends of the PEG arms. After reaction with ^{64}Cu, the nanotheranostic can be used for dual-modality imaging (MRI/PET) guided chemical therapy of tumor. The nanotheranostic exhibits higher levels of cellular uptake and tumor accumulation than those of its RGD-free counterpart. Lee and colleagues synthesized radiolabeled RGD peptide functionalized Er^{3+}/Yb^{3+} co-doped NaGdF$_4$ UCNPs (^{124}I-c(RGDyk)$_2$-UCNPs) by conjugation of the dimeric cyclic RGDyk ((cRGDyk)$_2$) peptide and PEG on polyacrylic acid-coated Er^{3+}/Yb^{3+} co-doped NaGdF$_4$ UCNPs and consecutively radiolabeled with ^{124}I [209]. The ^{124}I-c(RGDyk)$_2$-UCNPs have high specificity for $\alpha_v \beta_3$ integrin over-expressing U87MG tumor cells and mouse-bearing tumor model, which can be used as a PET/MR/UCL contrast agent with tumor angiogenesis-specific targeting properties. Zhao and colleagues synthesized CTX-functionalized Au PENPs by using polyethylenimine (PEI) as a template for conjugating PEG, glioma-specific peptide (chlorotoxin, CTX, RCLCQPGYCKGRGKGGCCDDCK-RAMQHDTTFCPMCM MCMPCFTTDHQMARKCDDCCGGKGRGKCYGPQCLCR-NH$_2$) and 3-(4-hydroxyphenyl)propionic acid-OSu (HPAO) and synthesizing 5 nm AuNPs [172]. After radiolabeling^{131}I via HPAO, the ^{131}I-labeled CTX-functionalized Au PENPs (^{131}I-Au PENPs-CTX) showed high radiochemical purity and stability, and could be used as a nanoprobe for the positive targeted SPECT/CT imaging and radionuclide therapy of glioma cells in vitro and in vivo in a mouse-bearing subcutaneous tumor. Due to the unique biological properties of CTX, the as-developed ^{131}I-Au PENPs-CTX were able to cross the blood–brain barrier (BBB) and specifically target glioma cells in a rat intracranial glioma model.

The peptide functionalized NPs have been extensively employed for targeting delivery chemodrugs from the injection site to their intracellular targets in tumorous cells [208,211–231]. Pan and colleagues have prepared monodispersed TAT peptide modified mesoporous silica NPs (MSNs-TAT) with high payload for nuclear-targeted drug delivery [211]. They found that MSNs-TAT with a diameter of 50 nm or smaller can efficiently target the nucleus and deliver the active anticancer drug DOX into the targeted nucleus, resulting in a significant enhancement in the anticancer activity of the drug. Ai and colleagues employed (pHLIP, NH$_2$-AAEQNPIYWARYADWLFTTPLLLLDLALLVDADEGTCG-COOH) to functionalize an 808 nm excited UCNP-based nanoplatform (pyropheophorbide (Ppa) loaded PEGylated UCNP) [228]. The pHLIP-functionalized nanoplatform exhibited an efficient 808 nm NIR laser-irradiated photodynamic therapy (PDT) effect in cancer cells, especially under a slightly acidic condition because the targeting properties of pHLIP to cancer cells under acidic conditions favor the entry of the nanoplatform. The in vivo experiment with a mouse-bearing breast tumor demonstrated that UCNPs were largely accumulated in the tumor site, revealing the excellent tumor-targeting properties of the pHLIP-functionalized nanoplatform, which ensures efficient PDT in vivo [223]. Recently, Xiao and colleagues synthesized a nanosystem (cRGD–PLGA–SPIO@DOX) based on cRGD peptide-functionalized poly(lactic-coglycolic acid) (cRGD–PLGA) block copolymer encapsulated DOX and SPIO for MRI-guided cancer therapy (as shown in Figure 9). The

cRGD–PLGA–SPIO@DOX exhibited improved antitumor effects and reduced toxicity compared with free DOX treatment and can act as a theranostic agent for real-time therapeutic monitoring [229].
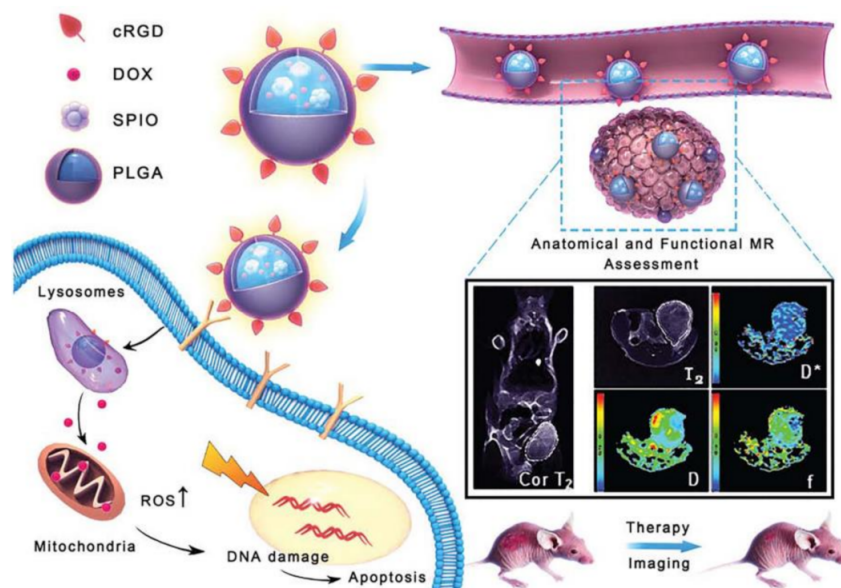
Figure 9. Schematic representation of the cRGD–PLGA–SPIO@DOX multifunctional NPs for targeted tumor therapy and MR imaging. The SPIO and DOX were encapsulated by cRGD peptide-functionalized poly(lactic-coglycolic acid) (cRGD–PLGA) block copolymer. The as-synthesized nanosystem (cRGD–PLGA–SPIO@DOX) exhibited excellent pH-responsive drug release properties under physiological conditions and integrin-targeting ability, which can act as a theranostic agent for MRI-guided cancer therapy (Adapted from Xiao et al. 2019 [229], Copyright 2019 The Royal Society of Chemistry and reproduced with permission.).

siRNA-based approach is one of the most promising new therapeutic strategies of cancer treatment, wherein siRNA can regulate the behavior of malignant tumor cells through manipulation of key oncogenes that modulate cellular signaling pathways [232]. The critical point of siRNA-based approach is delivery of the siRNA molecules with high selectivity and efficiency into tumor cells. Several peptide functionalized NP-based strategies have been developed for target-oriented delivery of siRNA with enhanced transfection efficiency [233–256]. As early as in 2010, Jung and colleagues studied the interactions of thiol-modified RGD tripeptide, thiol-modified HIV-Tat derived peptide, and EGFRvIII-targeting siRNA cofunctionalized CdSe/CdS/ZnS QDs with two brain cancer cells (U87 cells (overexpressing $\alpha_v\beta_3$) and PC 12 cells) [233]. They found that the RGD tripeptide functionalization led to higher cellular uptake of siRNA-QDs by the U87 cells than that by the PC-12 cells, resulting in significant decrease of the U87 cell viability. Due to excellent fluorescent property of QDs, the multifunctional siRNA-QDs can also be used for dissecting/tracking signaling cascades triggered by inhibiting specific proteins, showing great potential for simultaneous diagnosis, therapy, and prognosis of cancer. Veiseh and colleagues also confirmed that CTX functionalized SPIOs were well suited for targeted delivery of siRNA to brain cancer cells [234]. Due to their unique properties including pore-size tunability, large loading capacity, excellent biocompatibility, and easy surface modifiability, peptide functionalized mesoporous silica NPs (MSNs) have been demonstrated as promising nanocarriers for systemic delivery of siRNAs with high anticancer efficacy [236,237]. Li and colleagues reported a PEI and fusogenic peptide KALA-functionalized magnetic MSNs (M-MSNs)-based siRNA delivery system (M-MSN_siRNA@PEI-KALA) through the encapsulation of siRNA within the mesopores of M-MSNs, followed by the coating of PEI on the external surface of siRNA-loaded M-MSNs and the chemical conjugation of

KALA peptides [236]. Using anti-VEGF siRNA as a typical example, they demonstrated that the M-MSN_siRNA@PEI-KALA enabled to release the loaded siRNA into the cytoplasm and inhibit the tumor growth through the suppression of neovascularization in tumors. Zhu's group synthesized a series of RGDfC peptide functionalized selenium NP (SeNP)-based nanosystems for delivering different siRNAs with improved anticancer efficiency [239–243]. As shown in Figure 10a, the RGDfC-SeNPs exhibited excellent ability to deliver anti-Oct4 siRNA into HepG2 cells with high gene silencing efficacy (about 1.7 times of conventional lipofectamine 2000) [239]. The RGDfC-SeNPs/siRNA was specifically targeted to the HepG2 tumors and inhibited tumor growth significantly because they can selectively induce HepG2 cell apoptosis through silencing the Oct4 gene and arrested HepG2 cell at G2/M phase (as shown in Figure 10b). The RGDfC-SeNPs can also be used to co-delivery of DOX and siRNA [240]. The in vivo biodistribution experiment indicated that RGDfC-SeNPs@DOX/siRNA were capable of selectively accumulating in the tumor site, resulting in a higher anticancer activity than the free DOX, RGDfC-SeNPs@DOX, or RGDfC-SeNPs/siRNA in vitro and in vivo.
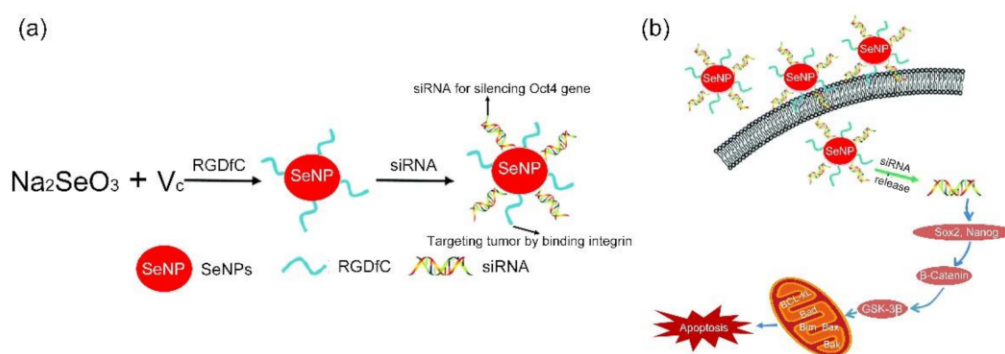
Figure 10. (**a**) Schematic representation of the formation of RGDfC-SeNPs/siRNA, and (**b**) the main signaling pathway of apoptosis induced by RGDfC-SeNPs/siRNA. The SeNPs were synthesized through reduction of Na_2SeO_3 by ascorbic acid (Vc), which were functionalized by the cancer-targeting ligand, RGDfC peptide. The siRNA was then loaded on the surface of RGDfC-SeNPs to prepare RGDfC-SeNPs/siRNA. The RGDfC-SeNPs/siRNA can induce cell apoptosis by regulating the Wnt/β-catenin signaling and activation of its downstream target gene (Adapted from Xia et al. 2017 [239], Copyright 2017 The Royal Society of Chemistry and reproduced with permission.).

The peptide functionalized NPs can also be used to deliver therapeutic peptides for tumor-targeting therapy [63,257]. As shown in Figure 11, Bian and colleagues developed a nanomedicine (termed as AuNp-DPA) based on small AuNPs (<10 nm in diameter) decorated with a D-peptide p53 activator (DPA, TAWYANFEALLR) coupled with polylysine (PLL) and receptor-targeted peptide (RGD[DP], CRGDKRGDSP) for targeted tumor therapy in vivo [257]. Take the advantages of the EPR effect and RGD targeting, the AuNP-DPA can successfully deliver DPA into cancer cells and specifically accumulate at tumor sites (as shown in Figure 11a). The results of in vitro and in vivo experiments demonstrated that small AuNP functionalized with therapeutic and targeting peptides has great potency for construction of biocompatible anticancer nanomedicine to overcome physiological and cellular barriers for targeted delivery of therapeutic D-peptides and further awaken their antitumor efficacy (as shown in Figure 11b).
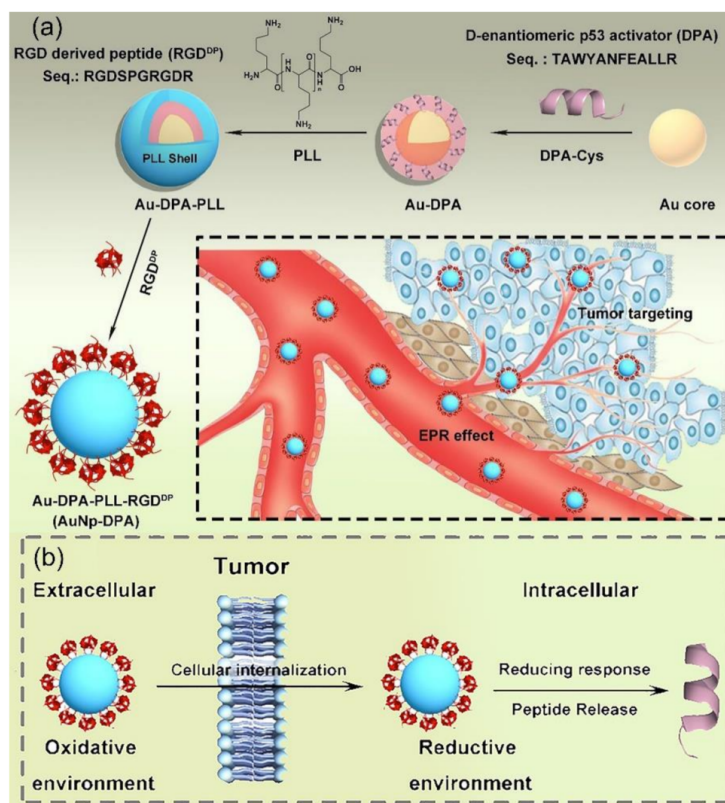
Figure 11. (**a**) Schematic depiction for the synthesis of AuNP-DPA and their enrichment in the tumor site. The AuNPs were modified by the C terminus of DPA (DPA-Cys, encapsulated by PLL, and functionalized by RGD-derived peptide RGDDP. (**b**) The AuNP-DPA can efficiently re-lease DPA to the cytosol through breaking the gold-thiolate bonds by the intracellular reductant, such as GSH. (Adapted from Bian et al. 2018 [257], Copyright 2018 Ivyspring International Pub-lisher and reproduced with permission.).

5. Conclusions and Future Prospects

In summary, the review discussed the recent progress of nanoplatforms based on peptide functionalized NPs for detection of cancer-related species and diagnosis and therapy of cancer. The combination of the advantages of NPs, such as high surface-area-to-volume ratio and unique optical/electrical/magnetic properties, and the structural and functional characteristics of peptides allows the peptide functionalized NP-based nanoplatforms to detect cancer markers with low LODs, and diagnosis and therapy of cancers with high efficiency. Although many excellent nanoplatforms based on peptide functionalized NPs have been developed during last two decades, only a few of them have used in clinical practices. For example, RGD functionalized GNRs for PTT of cancer has, by now, moved to the stage of preclinical testing.

Efficient clinical translation of the results of peptide functionalized NPs research requires continuous studies. For the in vitro detection, the peptide functionalized NP-based nanoplatforms should be performed in large scale of real samples and can be harmonized by the testing conditions. In addition, the features such as simplicity and cost should be considered since the remote areas lack laboratory equipment and well-trained people. For in vivo applications, the biodistribution, long-term toxicity, and pharmacokinetics of peptide functionalized NPs should be clearly addressed, which requires an auspicious understanding of the physicochemical properties of various peptide functionalized NPs at different nano/bio interfaces. For example, the nonbiodegradable NPs with large hydrodynamic size (more than 10 nm) exhibit long blood circulation half-life, which can significantly increase the time window of imaging and efficiency of therapy. The slow hepatobiliary excretion of large NPs also increases the likelihood of toxicity in vivo. In

order to solve this problem, it requires deep cooperation of scientists from different fields including biology, medicine, materials, chemistry, toxicology, pharmacy, and etc. to develop accurate standards/protocols for in vivo prediction/analysis of structure-toxicity relevance. The nano/bio interface studies could be accelerated by the use of high throughput screening methods and research achievements of bioinformatics on prediction of hazard and risk potential. Furthermore, the large-scale production and cost of manufacturing processes should be carefully considered, when the peptide functionalized NPs are used as nanomedicines, in particular as the drug delivery systems, for clinical applications. Although the development of peptide functionalized NP-based theranostics will face continued challenges, they hold great promise for combating cancers.

Author Contributions: Writing—original draft preparation, X.L., M.J., Q.Z., and Z.W.; writing—review and editing, X.L., Y.S., Q.Z., and Z.W. All authors have read and agreed to the published version of the manuscript.

Institutional Review Board Statement: Not applicable.

Informed Consent Statement: Not applicable.

Data Availability Statement: Not applicable.

Conflicts of Interest: The authors declare no conflict of interest.

Abbreviations

AgNPs: silver nanoparticles, AuNC: gold nanocluster, AuNPs: gold nanoparticles, AuNRs: gold nanorods, CAM: chorioallantoic membrane, CDs: carbon dots, CPPs: penetrating peptides, CRC: colorectal cancer, CT: Computed Tomography, CTX: chlorotoxin, CXCR4: CXC chemokine receptor 4, DIB-PEG-NH_2: 3,4-dihydroxy benzyl amine-poly(ethylene glycol)-NH_2, DOX: doxorubicin, EBV: Epstein-Barr virus, EDC/sulfo-NHS: 3-(ethyliminomethylideneamino)-N/N-dimethylpropan-1-amine/N-hydroxy sulfosuccinimide, EPR: enhanced permeability and retention, FI: fluorescein isothiocyanate, FRET: fluorescence resonance energy transfer, GEM: gemcitabine, GSH: glutathione, HDAC: histone deacetylase, HER2: human epidermal growth factor receptor 2, -HS: thiol group, IARC: International Agency for Research on Cancer, IONPs: iron oxide nanoparticles, LOD: detection limit, LSPR: localized surface plasmon resonance, MCP: monocyclic peptide, MET: metformin, MMP: matrix metalloproteinase, MnIO NPs: manganese-doped iron oxide nanoparticles, MR: magnetic resonance, MRI: magnetic resonance imaging, NES: nuclear export signal, NIR: near-infrared, NLS: nuclear localization signal, NPs: nanoparticles, OEG: oligoethyleneglycol, PADC: pancreatic ductal adenocarcinoma, PAMAM: poly(amidoamine) dendrimer, PDA: polydopamine, PEG: poly(ethylene glycol), PEI: polyethylenimine, PL: photoluminescence, PLGA: poly(lacticco-glycolic acid), PLL: polylysine, Ppa: pyropheophorbide, PSCs: perovskite solar cells, PTM: multiple posttranslational modification, PTP1B: protein tyrosine phosphatase 1B, PTT: photothermal therapy, PVDF: polyvinylidene fluoride, QDs: semiconductor quantum dots, SeNP: selenium nanoparticle, SERS: surface-enhanced resonant Raman scattering, siRNA: small-interfering RNA, SPIOs: superparamagnetic iron oxide nanoparticles, TAT: transactivator of transcription, TMB: 3,30,5,50-tetramethylbenzidine, TOPO: trioctylphosphine oxide, UCNPs: rare earth-doped up-conversion nanoparticles, VEGFR1: vascular endothelial growth factor receptor 1, WHO: World Health Organization, ZnONPs: zinc oxide nanoparticles, A (alanine, Ala), C (cysteine, Cys), D (aspartate, Asp), E (glutamic acid, Glu), F (phenylalanine, Phe), G (glycine, Gly), H (histidine, His), I (isoleucine, Ile), K (lysine, Lys), L (leucine, Leu), M (methionine, Met), N (asparagine, Asn), P (proline, Pro), Q (glutamine, Gln), R (arginine, Arg), S (serine, Ser), T (threonine, Thr), V (valine, Val), W (tryptophan, Trp), Y (tyrosine, Tyr), S(P) (phosphoseryl serine, Ser(P)).

References

1. Wild, C.; Weiderpass, E.; Stewart, B. *World Cancer Report: Cancer Research for Cancer Prevention*; Wild, C., Weiderpass, E., Stewart, B., Eds.; International Agency for Research on Cancer: Lyon, France, 2020; ISBN 978-92-832-0447-3.
2. Rosi, N.L.; Mirkin, C.A. Nanostructures in biodiagnostics. *Chem. Rev.* **2005**, *105*, 1547–1562. [CrossRef]
3. Wang, Z.X.; Ma, L.N. Gold nanoparticle probes. Coordin. *Chem. Rev.* **2009**, *253*, 1607–1618. [CrossRef]
4. Zhou, W.; Gao, X.; Liu, D.B.; Chen, X.Y. Gold Nanoparticles for In Vitro Diagnostics. *Chem. Rev.* **2015**, *115*, 10575–10636. [CrossRef] [PubMed]
5. Trouiller, A.J.; Hebie, S.; El Bahhaj, F.; Napporn, T.W.; Bertrand, P. Chemistry for oncotheranostic gold nanoparticles. *Eur. J. Med. Chem.* **2015**, *99*, 92–112. [CrossRef] [PubMed]
6. Chinen, A.B.; Guan, C.M.; Ferrer, J.R.; Barnaby, S.N.; Merkel, T.J.; Mirkin, C.A. Nanoparticle Probes for the Detection of Cancer Biomarkers, Cells, and Tissues by Fluorescence. *Chem. Rev.* **2015**, *115*, 10530–10574. [CrossRef]
7. Yang, D.M.; Ma, P.A.; Hou, Z.Y.; Cheng, Z.Y.; Li, C.X.; Lin, J. Current advances in lanthanide ion (Ln^{3+})-based upconversion nanomaterials for drug delivery. *Chem. Soc. Rev.* **2015**, *44*, 1416–1448. [CrossRef] [PubMed]
8. Zhu, X.J.; Su, Q.Q.; Feng, W.; Li, F.Y. Anti-Stokes shift luminescent materials for bio-applications. *Chem. Soc. Rev.* **2017**, *46*, 1025–1039. [CrossRef] [PubMed]
9. Dykman, L.A.; Khlebtsov, N.G. Multifunctional gold-based nanocomposites for theranostics. *Biomaterials* **2016**, *108*, 13–34. [CrossRef]
10. Zong, J.Y.; Cobb, S.L.; Cameron, N.R. Peptide-functionalized gold nanoparticles: Versatile biomaterials for diagnostic and therapeutic applications. *Biomater. Sci.* **2017**, *5*, 872–886. [CrossRef] [PubMed]
11. Tang, L.H.; Li, J.H. Plasmon-Based Colorimetric Nanosensors for Ultrasensitive Molecular Diagnostics. *ACS Sens.* **2017**, *2*, 857–875. [CrossRef]
12. Zhang, P.C.; Cui, Y.G.; Anderson, C.F.; Zhang, C.L.; Li, Y.P.; Wang, R.F.; Cui, H.G. Peptide-based nanoprobes for molecular imaging and disease diagnostics. *Chem. Soc. Rev.* **2018**, *47*, 3490–3529. [CrossRef] [PubMed]
13. Chakraborty, A.; Boer, J.C.; Selomulya, C.; Plebanski, M. Amino Acid Functionalized Inorganic Nanoparticles as Cutting-Edge Therapeutic and Diagnostic Agents. *Bioconjugate Chem.* **2018**, *29*, 657–671. [CrossRef] [PubMed]
14. Spicer, C.D.; Jumeaux, C.; Gupta, B.; Stevens, M.M. Peptide and protein nanoparticle conjugates: Versatile platforms for biomedical applications. *Chem. Soc. Rev.* **2018**, *47*, 3574–3620. [CrossRef] [PubMed]
15. Zhang, Y.; Zhang, C.Y.; Xu, C.; Wang, X.L.; Liu, C.; Waterhouse, G.I.N.; Wang, Y.L.; Yin, H.Z. Ultrasmall Au nanoclusters for biomedical and biosensing applications: A mini-review. *Talanta* **2019**, *200*, 432–442. [CrossRef] [PubMed]
16. Zhu, D.D.; Hu, C.L.; Liu, Y.; Chen, F.; Zheng, Z.; Wang, X.L. Enzyme-/Redox-Responsive Mesoporous Silica Nanoparticles Based on Functionalized Dopamine as Nanocarriers for Cancer Therapy. *ACS Omega* **2019**, *4*, 6097–6105. [CrossRef]
17. Mohebbi, S.; Moghadam, T.T.; Nikkhah, M.; Behmanesh, M. RGD-HK Peptide-Functionalized Gold Nanorods Emerge as Targeted Biocompatible Nanocarriers for Biomedical Applications. *Nanoscale Res. Lett.* **2019**, *14*, 13. [CrossRef] [PubMed]
18. Zhang, Q.Y.; Liang, J.Y.; Yun, S.L.J.; Liang, K.; Yang, D.Y.; Gu, Z. Recent advances in improving tumor-targeted delivery of imaging nanoprobes. *Biomater. Sci.* **2020**, *8*, 4129–4146. [CrossRef]
19. Pigliacelli, C.; Sanchez-Fernandez, R.; Garcia, M.D.; Peinador, C.; Pazos, E. Self-assembled peptide-inorganic nanoparticle superstructures: From component design to applications. *Chem. Commun.* **2020**, *56*, 8000–8014. [CrossRef]
20. Liu, X.H.; Zhang, Q.W.; Knoll, W.G.; Liedberg, B.; Wang, Y. Rational Design of Functional Peptide-Gold Hybrid Nanomaterials for Molecular Interactions. *Adv. Mater.* **2020**, *32*, 2000866. [CrossRef]
21. Sun, D.X.; Zhou, S.; Gao, W. What Went Wrong with Anticancer Nanomedicine Design and How to Make It Right. *ACS Nano* **2020**, *14*, 12281–12290. [CrossRef]
22. Chung, Y.J.; Kim, J.; Park, C.B. Photonic Carbon Dots as an Emerging Nanoagent for Biomedical and Healthcare Applications. *ACS Nano* **2020**, *14*, 6470–6497. [CrossRef]
23. Liu, J.J.; Li, R.; Yang, B. Carbon Dots: A New Type of Carbon-Based Nanomaterial with Wide Applications. *ACS Cent. Sci.* **2020**, *6*, 2179–2195. [CrossRef]
24. Lai, W.F.; Wong, W.T.; Rogach, A.L. Development of Copper Nanoclusters for In Vitro and In Vivo Theranostic Applications. *Adv. Mater.* **2020**, *32*, 1906872. [CrossRef]
25. Quintana, C.; Cifuentes, M.P.; Humphrey, M.G. Transition metal complex/gold nanoparticle hybrid materials. *Chem. Soc. Rev.* **2020**, *49*, 2316–2341. [CrossRef]
26. Nel, A.E. Transformational Impact of Nanomedicine: Reconciling Outcome with Promise. *Nano Lett.* **2020**, *20*, 5601–5603. [CrossRef]
27. Shahbazi, M.A.; Faghfouri, L.; Ferreira, M.P.A.; Figueiredo, P.; Maleki, H.; Sefat, F.; Hirvonen, J.; Santos, H.A. The versatile biomedical applications of bismuth-based nanoparticles and composites: Therapeutic, diagnostic, biosensing, and regenerative properties. *Chem. Soc. Rev.* **2020**, *49*, 1253–1321. [CrossRef] [PubMed]
28. Li, Z.; Xiao, C.; Yong, T.Y.; Li, Z.F.; Gan, L.; Yang, X.L. Influence of nanomedicine mechanical properties on tumor targeting delivery. *Chem. Soc. Rev.* **2020**, *49*, 2273–2290. [CrossRef] [PubMed]
29. Wang, H.X.; Wu, T.T.; Li, M.Q.; Tao, Y. Recent advances in nanomaterials for colorimetric cancer detection. *J. Mater. Chem. B.* **2021**, *9*, 921–938. [CrossRef] [PubMed]

30. Wong, X.Y.; Sena-Torralba, A.; Alvarez-Diduk, R.; Muthoosamy, K.; Merkoci, A. Nanomaterials for Nanotheranostics: Tuning Their Properties According to Disease Needs. *ACS Nano* **2020**, *14*, 2585–2627. [CrossRef]

31. Kandell, R.M.; Waggoner, L.E.; Kwon, E.J. Nanomedicine for Acute Brain Injuries: Insight from Decades of Cancer Nanomedicine. *Mol. Pharm.* **2021**, *18*, 522–538. [CrossRef]

32. Maeda, H. The 35th Anniversary of the Discovery of EPR Effect: A New Wave of Nanomedicines for Tumor-Targeted Drug Delivery—Personal Remarks and Future Prospects. *J. Pers. Med.* **2021**, *11*, 229. [CrossRef]

33. Li, X.D.; Sun, Y.H.; Ma, L.N.; Liu, G.F.; Wang, Z.X. The Renal Clearable Magnetic Resonance Imaging Contrast Agents: State of the Art and Recent Advances. *Molecules* **2020**, *25*, 5072. [CrossRef]

34. Desale, K.; Kuche, K.; Jain, S. Cell-penetrating peptides (CPPs): An overview of applications for improving the potential of nanotherapeutics. *Biomater. Sci.* **2021**, *9*, 1153–1188. [CrossRef]

35. Malonis, R.J.; Lai, J.R.; Vergnolle, O. Peptide-Based Vaccines: Current Progress and Future Challenges. *Chem. Rev.* **2020**, *120*, 3210–3229. [CrossRef] [PubMed]

36. Lenci, E.; Trabocchi, A. Peptidomimetic toolbox for drug discovery. *Chem. Soc. Rev.* **2020**, *49*, 3262–3277. [CrossRef] [PubMed]

37. Pierschbacher, M.D.; Ruoslahti, E. Cell Attachment Activity of Fibronectin Can Be Duplicated by Small Synthetic Fragments of the Molecule. *Nature* **1984**, *309*, 30–33. [CrossRef] [PubMed]

38. Nieberler, M.; Reuning, U.; Reichart, F.; Notni, J.; Wester, H.J.; Schwaiger, M.; Weinmuller, M.; Rader, A.; Steiger, K.; Kessler, H. Exploring the Role of RGD-Recognizing Integrins in Cancer. *Cancers* **2017**, *9*, 116. [CrossRef]

39. Morshed, R.A.; Muroski, M.E.; Dai, Q.; Wegscheid, M.L.; Auffinger, B.; Yu, D.; Han, Y.; Zhang, L.J.; Wu, M.J.; Cheng, Y.; et al. Cell-Penetrating Peptide-Modified Gold Nanoparticles for the Delivery of Doxorubicin to Brain Metastatic Breast Cancer. *Mol. Pharm.* **2016**, *13*, 1843–1854. [CrossRef] [PubMed]

40. Li, Y.; Tang, Z.H.; Prasad, P.N.; Knecht, M.R.; Swihart, M.T. Peptide-mediated synthesis of gold nanoparticles: Effects of peptide sequence and nature of binding on physicochemical properties. *Nanoscale* **2014**, *6*, 3165–3172. [CrossRef]

41. Wang, W.; Anderson, C.F.; Wang, Z.Y.; Wu, W.; Cui, H.G.; Liu, C.J. Peptide-templated noble metal catalysts: Syntheses and applications. *Chem. Sci.* **2017**, *8*, 3310–3324. [CrossRef]

42. Levy, R.; Thanh, N.T.K.; Doty, R.C.; Hussain, I.; Nichols, R.J.; Schiffrin, D.J.; Brust, M.; Fernig, D.G. Rational and combinatorial design of peptide capping Ligands for gold nanoparticles. *J. Am. Chem. Soc.* **2004**, *126*, 10076–10084. [CrossRef] [PubMed]

43. Wang, Z.; Levy, R.; Fernig, D.G.; Brust, M. The peptide route to multifunctional gold nanoparticles. *Bioconjugate Chem.* **2005**, *16*, 497–500. [CrossRef]

44. Krpetic, Z.; Nativo, P.; Porta, F.; Brust, M. A Multidentate Peptide for Stabilization and Facile Bioconjugation of Gold Nanoparticles. *Bioconjugate Chem.* **2009**, *20*, 619–624. [CrossRef]

45. Krpetic, Z.; Saleemi, S.; Prior, I.A.; See, V.; Qureshi, R.; Brust, M. Negotiation of Intracellular Membrane Barriers by TAT-Modified Gold Nanoparticles. *ACS Nano* **2011**, *5*, 5195–5201. [CrossRef] [PubMed]

46. Yang, J.; Yao, M.H.; Du, M.S.; Jin, R.M.; Zhao, D.H.; Ma, J.; Ma, Z.Y.; Zhao, Y.D.; Liu, B. A near-infrared light-controlled system for reversible presentation of bioactive ligands using polypeptide-engineered functionalized gold nanorods. *Chem. Commun.* **2015**, *51*, 2569–2572. [CrossRef]

47. Fernandes, R.; Smyth, N.R.; Muskens, O.L.; Nitti, S.; Heuer-Jungemann, A.; Ardern-Jones, M.R.; Kanaras, A.G. Interactions of Skin with Gold Nanoparticles of Different Surface Charge, Shape, and Functionality. *Small* **2015**, *11*, 713–721. [CrossRef] [PubMed]

48. Colangelo, E.; Chen, Q.B.; Davidson, A.M.; Paramelle, D.; Sullivan, M.B.; Volk, M.; Levy, R. Computational and Experimental Investigation of the Structure of Peptide Monolayers on Gold Nanoparticles. *Langmuir* **2017**, *33*, 438–449. [CrossRef]

49. Natarajan, P.; Sukthankar, P.; Changstrom, J.; Holland, C.S.; Barry, S.; Hunter, W.B.; Sorensen, C.M.; Tomich, J.M. Synthesis and Characterization of Multifunctional Branched Amphiphilic Peptide Bilayer Conjugated Gold Nanoparticles. *ACS Omega* **2018**, *3*, 11071–11083. [CrossRef]

50. Monti, S.; Barcaro, G.; Sementa, L.; Carravetta, V.; Agren, H. Dynamics and self-assembly of bio-functionalized gold nanoparticles in solution: Reactive molecular dynamics simulations. *Nano Res.* **2018**, *11*, 1757–1767. [CrossRef]

51. Samieegohar, M.; Sha, F.; Clayborne, A.Z.; Wei, T. ReaxFF MD Simulations of Peptide-Grafted Gold Nanoparticles. *Langmuir* **2019**, *35*, 5029–5036. [CrossRef]

52. Luo, J.; Cheng, Y.; Gong, Z.W.; Wu, K.; Zhou, Y.; Chen, H.X.; Gauthier, M.; Cheng, Y.Z.; Liang, J.; Zou, T. Self-Assembled Peptide Functionalized Gold Nanopolyhedrons with Excellent Chiral Optical Properties. *Langmuir* **2020**, *36*, 600–608. [CrossRef] [PubMed]

53. Hu, B.; Kong, F.P.; Gao, X.N.; Jiang, L.L.; Li, X.F.; Gao, W.; Xu, K.H.; Tang, B. Avoiding Thiol Compound Interference: A Nanoplatform Based on High-Fidelity Au-Se Bonds for Biological Applications. *Angew. Chem. Int. Ed.* **2018**, *57*, 5306–5309. [CrossRef]

54. Luan, M.M.; Shi, M.W.; Pan, W.; Li, N.; Tang, B. A gold-selenium-bonded nanoprobe for real-time in situ imaging of the upstream and downstream relationship between uPA and MMP-9 in cancer cells. *Chem. Commun.* **2019**, *55*, 5817–5820. [CrossRef] [PubMed]

55. Pan, W.; Liu, X.H.; Wan, X.Y.; Li, J.; Li, Y.H.; Lu, F.; Li, N.; Tang, B. Rapid Preparation of Au-Se-Peptide Nanoprobe Based on a Freezing Method for Bioimaging. *Anal. Chem.* **2019**, *91*, 15982–15987. [CrossRef] [PubMed]

56. Liu, F.Y.; He, X.X.; Zhang, J.P.; Zhang, H.M.; Wang, Z.X. Employing Tryptone as a General Phase Transfer Agent to Produce Renal Clearable Nanodots for Bioimaging. *Small* **2015**, *11*, 3676–3685. [CrossRef]

57. Chen, H.D.; Li, X.D.; Liu, F.Y.; Zhang, H.M.; Wang, Z.X. Renal Clearable Peptide Functionalized NaGdF$_4$ Nanodots for High-Efficiency Tracking Orthotopic Colorectal Tumor in Mouse. *Mol. Pharm.* **2017**, *14*, 3134–3141. [CrossRef]

58. Bartczak, D.; Kanaras, A.G. Preparation of Peptide-Functionalized Gold Nanoparticles Using One Pot EDC/Sulfo-NHS Coupling. *Langmuir* **2011**, *27*, 10119–10123. [CrossRef]

59. Roma-Rodrigues, C.; Heuer-Jungemann, A.; Fernandes, A.R.; Kanaras, A.G.; Baptista, P.V. Peptide-coated gold nanoparticles for modulation of angiogenesis in vivo. *Int. J. Nanomed.* **2016**, *11*, 2633–2639. [CrossRef]

60. Nicolardi, S.; van der Burgt, Y.E.M.; Codee, J.D.C.; Wuhrer, M.; Hokke, C.H.; Chiodo, F. Structural Characterization of Biofunctionalized Gold Nanoparticles by Ultrahigh-Resolution Mass Spectrometry. *ACS Nano* **2017**, *11*, 8257–8264. [CrossRef]

61. Wilder, L.M.; Fies, W.A.; Rabin, C.; Webb, L.J.; Crooke, R.M. Conjugation of an alpha-Helical Peptide to the Surface of Gold Nanoparticles. *Langmuir* **2019**, *35*, 3363–3371. [CrossRef]

62. Fu, Y.; Li, X.; Chen, H.; Wang, Z.; Yang, W.; Zhang, H. CXC Chemokine Receptor 4 Antagonist Functionalized Renal Clearable Manganese-Doped Iron Oxide Nanoparticles for Active-Tumor-Targeting Magnetic Resonance Imaging-Guided Bio-Photothermal Therapy. *ACS Appl. Bio Mater.* **2019**, *2*, 3613–3621. [CrossRef]

63. Zhang, W.T.; Liu, X.F.; Zhao, X.N.; Zhang, X.F. Controllable delivery of peptides by superparamagnetic Fe$_3$O$_4$/slica nanoparticle vehicles. *Mater. Lett.* **2017**, *201*, 177–180. [CrossRef]

64. Li, X.X.; Liu, L.; Fu, Y.; Chen, H.D.; Abualrejal, M.M.A.; Zhang, H.; Wang, Z.X.; Zhang, H.M. Peptide-enhanced tumor accumulation of upconversion nanoparticles for sensitive upconversion luminescence/magnetic resonance dual-mode bioimaging of colorectal tumors. *Acta Biomater.* **2020**, *104*, 167–175. [CrossRef]

65. Liu, L.; Li, X.T.; Zhang, H.; Chen, H.D.; Abualrejal, M.M.A.; Song, D.Q.; Wang, Z.X. Six-in-one peptide functionalized upconversion@polydopamine nanoparticle-based ratiometric fluorescence sensing platform for real-time evaluating anticancer efficacy through monitoring caspase-3 activity. *Sens. Actuator B Chem.* **2021**, *333*, 129554. [CrossRef]

66. Si, S.; Mandal, T.K. Tryptophan-based peptides to synthesize gold and silver nanoparticles: A mechanistic and kinetic study. *Chem. Eur. J.* **2007**, *13*, 3160–3168. [CrossRef] [PubMed]

67. Graf, P.; Mantion, A.; Foelske, A.; Shkilnyy, A.; Masic, A.; Thunemann, A.E.; Taubert, A. Peptide-Coated Silver Nanoparticles: Synthesis, Surface Chemistry, and pH-Triggered, Reversible Assembly into Particle Assemblies. *Chem. Eur. J.* **2009**, *15*, 5831–5844. [CrossRef] [PubMed]

68. Upert, G.; Bouillere, F.; Wennemers, H. Oligoprolines as Scaffolds for the Formation of Silver Nanoparticles in Defined Sizes: Correlating Molecular and Nanoscopic Dimensions. *Angew. Chem. Int. Ed.* **2012**, *51*, 4231–4234. [CrossRef]

69. Fanelli, R.; Milli, L.; Cornia, A.; Moretto, A.; Castellucci, N.; Zanna, N.; Malachin, G.; Tavano, R.; Tomasini, C. Chiral Gold Nanoparticles Decorated with Pseudopeptides. *Eur. J. Org. Chem.* **2015**, *2015*, 6243–6248. [CrossRef]

70. Papst, S.; Brimble, M.A.; Tilley, R.D.; Williams, D.E. One-Pot Synthesis of Functionalized Noble Metal Nanoparticles Using a Rationally Designed Phosphopeptide. *Part. Part. Syst. Char.* **2014**, *31*, 971–975. [CrossRef]

71. Corra, S.; Lewandowska, U.; Benetti, E.M.; Wennemers, H. Size-Controlled Formation of Noble-Metal Nanoparticles in Aqueous Solution with a Thiol-Free Tripeptide. *Angew. Chem. Int. Ed.* **2016**, *55*, 8542–8545. [CrossRef] [PubMed]

72. Si, S.; Kotal, A.; Mandal, T.K. One-dimensional assembly of peptide-functionalized gold nanoparticles: An approach toward mercury ion sensing. *J. Phys. Chem. C* **2007**, *111*, 1248–1255. [CrossRef]

73. Li, X.K.; Wang, J.N.; Sun, L.L.; Wang, Z.X. Gold nanoparticle-based colorimetric assay for selective detection of aluminium cation on living cellular surfaces. *Chem. Commun.* **2010**, *46*, 988–990. [CrossRef] [PubMed]

74. Zhu, D.R.; Li, X.K.; Liu, X.; Wang, J.N.; Wang, Z.X. Designing bifunctionalized gold nanoparticle for colorimetric detection of Pb^{2+} under physiological condition. *Biosens. Bioelectron.* **2012**, *31*, 505–509. [CrossRef]

75. Chen, H.X.; Zhang, J.J.; Liu, X.J.; Gao, Y.M.; Ye, Z.H.; Li, G.X. Colorimetric copper(II) ion sensor based on the conformational change of peptide immobilized onto the surface of gold nanoparticles. *Anal. Methods* **2014**, *6*, 2580–2585. [CrossRef]

76. Yu, Y.M.; Hong, Y.; Gao, P.; Nazeeruddin, M.K. Glutathione Modified Gold Nanoparticles for Sensitive Colorimetric Detection of Pb^{2+} Ions in Rainwater Polluted by Leaking Perovskite Solar Cells. *Anal. Chem.* **2016**, *88*, 12316–12322. [CrossRef]

77. Li, X.Y.; Wu, Z.T.; Zhou, X.D.; Hu, J.M. Colorimetric response of peptide modified gold nanoparticles: An original assay for ultrasensitive silver detection. *Biosens. Bioelectron.* **2017**, *92*, 496–501. [CrossRef]

78. Shinde, S.; Kim, D.Y.; Saratale, R.G.; Syed, A.; Ameen, F.; Ghodake, G. A Spectral Probe for Detection of Aluminum (III) Ions Using Surface Functionalized Gold Nanoparticles. *Nanomaterials* **2017**, *7*, 287. [CrossRef] [PubMed]

79. Parnsubsakul, A.; Oaew, S.; Surareungchai, W. Zwitterionic peptide-capped gold nanoparticles for colorimetric detection of Ni^{2+}. *Nanoscale* **2018**, *10*, 5466–5473. [CrossRef] [PubMed]

80. Zhou, G.H.; Liu, Y.Z.; Luo, M.; Xu, Q.F.; Ji, X.H.; He, Z.K. Peptide-Capped Gold Nanoparticle for Colorimetric Immunoassay of Conjugated Abscisic Acid. *ACS Appl. Mater. Interfaces* **2012**, *4*, 5010–5015. [CrossRef] [PubMed]

81. Wei, L.M.; Wang, X.Y.; Li, C.; Li, X.X.; Yin, Y.M.; Li, G.X. Colorimetric assay for protein detection based on "nano-pumpkin" induced aggregation of peptide-decorated gold nanoparticles. *Biosens. Bioelectron.* **2015**, *71*, 348–352. [CrossRef]

82. Feng, T.T.; Gao, S.Q.; Wang, K. Colorimetric Sensing of Prostate Specific Membrane Antigen Based on Gold Nanoparticles. *Acta Chim. Sin.* **2019**, *77*, 422–426. [CrossRef]

83. Retout, M.; Valkenier, H.; Triffaux, E.; Doneux, T.; Bartik, K.; Bruylants, G. Rapid and Selective Detection of Proteins by Dual Trapping Using Gold Nanoparticles Functionalized with Peptide Aptamers. *ACS Sens.* **2016**, *1*, 929–933. [CrossRef]

84. Liu, X.H.; Wang, Y.; Chen, P.; McCadden, A.; Palaniappan, A.; Zhang, J.L.; Liedberg, B. Peptide Functionalized Gold Nanoparticles with Optimized Particle Size and Concentration for Colorimetric Assay Development: Detection of Cardiac Troponin I. *ACS Sens.* **2016**, *1*, 1416–1422. [CrossRef]

85. Wang, Z.X.; Levy, R.; Fernig, D.G.; Brust, M. Kinase-catalyzed modification of gold nanoparticles: A new approach to colorimetric kinase activity screening. *J. Am. Chem. Soc.* **2006**, *128*, 2214–2215. [CrossRef]

86. Gupta, S.; Andresen, H.; Ghadiali, J.E.; Stevens, M.M. Kinase-Actuated Immunoaggregation of Peptide-Conjugated Gold Nanoparticles. *Small* **2010**, *6*, 1509–1513. [CrossRef]

87. Huang, H.; Zhang, Q.W.; Luo, J.X.; Zhao, Y. Sensitive colorimetric detection of lysozyme in human serum using peptide-capped gold nanoparticles. *Anal. Methods* **2012**, *4*, 3874–3878. [CrossRef]

88. Chen, P.; Selegard, R.; Aili, D.; Liedberg, B. Peptide functionalized gold nanoparticles for colorimetric detection of matrilysin (MMP-7) activity. *Nanoscale* **2013**, *5*, 8973–8976. [CrossRef] [PubMed]

89. Liu, X.H.; Wang, Y.; Chen, P.; Wang, Y.S.; Mang, J.L.; Aili, D.; Liedberg, B. Biofunctionalized Gold Nanoparticles for Colorimetric Sensing of Botulinum Neurotoxin A Light Chain. *Anal. Chem.* **2014**, *86*, 2345–2352. [CrossRef]

90. Chandrawati, R.; Stevens, M.M. Controlled assembly of peptide-functionalized gold nanoparticles for label-free detection of blood coagulation Factor XIII activity. *Chem. Commun.* **2014**, *50*, 5431–5434. [CrossRef] [PubMed]

91. Lee, J.O.; Kim, E.J.; Lim, B.; Kim, T.W.; Kim, Y.P. Rapid Detection of Protein Phosphatase Activity Using Zn(II)Coordinated Gold Nanosensors Based on His-Tagged Phosphopeptides. *Anal. Chem.* **2015**, *87*, 1257–1265. [CrossRef] [PubMed]

92. Sun, S.J.; Shen, H.X.; Liu, C.H.; Li, Z.P. Phosphorylation-regulated crosslinking of gold nanoparticles: A new strategy for colorimetric detection of protein kinase activity. *Analyst* **2015**, *140*, 5685–5691. [CrossRef]

93. Xia, N.; Wang, X.; Wang, X.J.; Zhou, B.B. Gold Nanoparticle-Based Colorimetric and Electrochemical Methods for Dipeptidyl Peptidase-IV Activity Assay and Inhibitor Screening. *Materials* **2016**, *9*, 857. [CrossRef] [PubMed]

94. Aldewachi, H.S.; Woodroofe, N.; Turega, S.; Gardiner, P.H.E. Optimization of gold nanoparticle-based real-time colorimetric assay of dipeptidyl peptidase IV activity. *Talanta* **2017**, *169*, 13–19. [CrossRef]

95. Mao, X.X.; Li, Y.F.; Han, P.; Wang, X.H.; Yang, S.Q.; Zhang, F.; Gong, X.Q.; Cao, Y. One-pot and one-step colorimetric detection of aminopeptidase N activity based on gold nanoparticles-based supramolecular structure. *Sens. Actuator B Chem.* **2018**, *267*, 336–341. [CrossRef]

96. Aldewachi, H.; Woodroofe, N.; Gardiner, P. Study of the Stability of Functionalized Gold Nanoparticles for the Colorimetric Detection of Dipeptidyl Peptidase IV. *Appl. Sci.* **2018**, *8*, 2589. [CrossRef]

97. Loynachan, C.N.; Soleimany, A.P.; Dudani, J.S.; Lin, Y.Y.; Najer, A.; Bekdemir, A.; Chen, Q.; Bhatia, S.N.; Stevens, M.M. Renal clearable catalytic gold nanoclusters for in vivo disease monitoring. *Nat. Nanotechnol.* **2019**, *14*, 883–890. [CrossRef] [PubMed]

98. Goyal, G.; Palaniappan, A.; Liedberg, B. Protease functional assay on membrane. *Sens. Actuator B Chem.* **2020**, *305*, 127442. [CrossRef]

99. Gao, L.; Liu, M.Q.; Ma, G.F.; Wang, Y.L.; Zhao, L.N.; Yuan, Q.; Gao, F.P.; Liu, R.; Zhai, J.; Chai, Z.F.; et al. Peptide-Conjugated Gold Nanoprobe: Intrinsic Nanozyme-Linked Immunsorbant Assay of Integrin Expression Level on Cell Membrane. *ACS Nano* **2015**, *9*, 10979–10990. [CrossRef]

100. Feng, J.Y.; Huang, P.C.; Shi, S.Z.; Deng, K.Y.; Wu, F.Y. Colorimetric detection of glutathione in cells based on peroxidase-like activity of gold nanoclusters: A promising powerful tool for identifying cancer cells. *Anal. Chim. Acta.* **2017**, *967*, 64–69. [CrossRef] [PubMed]

101. Wang, X.H.; Geng, J.; Miyoshi, D.; Ren, J.S.; Sugimoto, N.; Qu, X.G. A rapid and sensitive "add-mix-measure" assay for multiple proteinases based on one gold nanoparticle-peptide-fluorophore conjugate. *Biosens. Bioelectron.* **2010**, *26*, 743–747. [CrossRef]

102. Wang, Y.; Liu, X.H.; Zhang, J.L.; Aili, D.; Liedberg, B. Time-resolved botulinum neurotoxin A activity monitored using peptide-functionalized Au nanoparticle energy transfer sensors. *Chem. Sci.* **2014**, *5*, 2651–2656. [CrossRef]

103. Wang, M.K.; Wang, L.; Liu, Q.; Su, X.G. A fluorescence sensor for protein kinase activity detection based on gold nanoparticles/copper nanoclusters system. *Sens. Actuator B Chem.* **2018**, *256*, 691–698. [CrossRef]

104. Xu, S.M.; Zhang, F.M.; Xu, L.B.; Liu, X.; Ma, P.Y.; Sun, Y.; Wang, X.H.; Song, D.Q. A fluorescence resonance energy transfer biosensor based on carbon dots and gold nanoparticles for the detection of trypsin. *Sens. Actuator B Chem.* **2018**, *273*, 1015–1021. [CrossRef]

105. Zhang, D.D.; Meng, Y.R.; Zhang, C.Y. Peptide-templated gold nanoparticle nanosensor for simultaneous detection of multiple posttranslational modification enzymes. *Chem. Commun.* **2020**, *56*, 213–216. [CrossRef]

106. Wang, Y.H.; Shen, P.; Li, C.Y.; Wang, Y.Y.; Liu, Z.H. Upconversion Fluorescence Resonance Energy Transfer Based Biosensor for Ultrasensitive Detection of Matrix Metalloproteinase-2 in Blood. *Anal. Chem.* **2012**, *84*, 1466–1473. [CrossRef]

107. Vuojola, J.; Riuttamaki, T.; Kulta, E.; Arppe, R.; Soukka, T. Fluorescence-quenching-based homogeneous caspase-3 activity assay using photon upconversion. *Anal. Chim. Acta.* **2012**, *725*, 67–73. [CrossRef]

108. Zeng, T.; Zhang, T.; Wei, W.; Li, Z.; Wu, D.; Wang, L.; Guo, J.; He, X.W.; Ma, N. Compact, Programmable, and Stable Biofunctionalized Upconversion Nanoparticles Prepared through Peptide-Mediated Phase Transfer for High-Sensitive Protease Sensing and in Vivo Apoptosis Imaging. *ACS Appl. Mater. Interfaces* **2015**, *7*, 11849–11856. [CrossRef] [PubMed]

109. Wu, M.M.; Wang, X.Y.; Wang, K.; Guo, Z.J. An ultrasensitive fluorescent nanosensor for trypsin based on upconversion nanoparticles. *Talanta* **2017**, *174*, 797–802. [CrossRef] [PubMed]

110. Chen, H.Y.; Fang, A.J.; Zhang, Y.Y.; Yao, S.Z. Silver triangular nanoplates as an high efficiently FRET donor-acceptor of upconversion nanoparticles for ultrasensitive "Turn on-off" protamine and trypsin sensor. *Talanta* **2017**, *174*, 148–155. [CrossRef] [PubMed]

111. Cao, S.N.; Li, Z.; Zhao, J.Y.; Chen, M.; Ma, N. Rational Engineering a Multichannel Upconversion Sensor for Multiplex Detection of Matrix Metalloproteinase Activities. *ACS Sens.* **2018**, *3*, 1522–1530. [CrossRef] [PubMed]

112. Chan, Y.C.; Chan, M.H.; Chen, C.W.; Liu, R.S.; Hsiao, M.; Tsai, D.P. Near-Infrared-Activated Fluorescence Resonance Energy Transfer-Based Nanocomposite to Sense MMP2-Overexpressing Oral Cancer Cells. *ACS Omega* **2018**, *3*, 1627–1634. [CrossRef] [PubMed]

113. Liu, L.; Zhang, H.; Song, D.Q.; Wang, Z.X. An upconversion nanoparticle-based fluorescence resonance energy transfer system for effectively sensing caspase-3 activity. *Analyst* **2018**, *143*, 761–767. [CrossRef]

114. Liu, L.; Zhang, H.; Wang, Z.X.; Song, D.Q. Peptide-functionalized upconversion nanoparticles-based FRET sensing platform for Caspase-9 activity detection in vitro and in vivo. *Biosens. Bioelectron.* **2019**, *141*, 111403. [CrossRef]

115. Jung, S.; Chen, X.Y. Quantum Dot-Dye Conjugates for Biosensing, Imaging, and Therapy. *Adv. Healthc. Mater.* **2018**, *7*, 1800252. [CrossRef] [PubMed]

116. Lei, Z.; Jian, M.H.; Li, X.T.; Wei, J.; Meng, X.Y.; Wang, Z.X. Biosensors and bioassays for determination of matrix metalloproteinases: State of the art and recent advances. *J. Mater. Chem. B* **2020**, *8*, 3261–3291. [CrossRef]

117. Dos Santos, M.C.; Algar, W.R.; Medintz, I.L.; Hildebrandt, N. Quantum dots for Forster Resonance Energy Transfer FRET. *TrAC-Trends Anal. Chem.* **2020**, *125*, 115819. [CrossRef]

118. Tong, X.; Shi, S.Y.; Tong, C.Y.; Iftikhar, A.; Long, R.Q.; Zhu, Y.F. Quantum/carbon dots-based fluorescent assays for enzyme activity. *TrAC-Trends Anal. Chem.* **2020**, *131*, 116008. [CrossRef]

119. Chern, M.; Toufanian, R.; Dennis, A.M. Quantum dot to quantum dot Forster resonance energy transfer: Engineering materials for visual color change sensing. *Analyst* **2020**, *145*, 5754–5767. [CrossRef]

120. Arndt, N.; Tran, H.D.N.; Zhang, R.; Xu, Z.P.; Ta, H.T. Different Approaches to Develop Nanosensors for Diagnosis of Diseases. *Adv. Sci.* **2020**, *7*, 2001476. [CrossRef]

121. Shi, L.F.; De Paoli, V.; Rosenzweig, N.; Rosenzweig, Z. Synthesis and application of quantum dots FRET-based protease sensors. *J. Am. Chem. Soc.* **2006**, *128*, 10378–10379. [CrossRef]

122. Medintz, I.L.; Clapp, A.R.; Brunel, F.M.; Tiefenbrunn, T.; Uyeda, H.T.; Chang, E.L.; Deschamps, J.R.; Dawson, P.E.; Mattoussi, H. Proteolytic activity monitored by fluorescence resonance energy transfer through quantum-dot-peptide conjugates. *Nat. Mater.* **2006**, *5*, 581–589. [CrossRef]

123. Lin, S.Y.; Chen, N.T.; Sun, S.P.; Chang, J.C.; Wang, Y.C.; Yang, C.S.; Lo, L.W. The Protease-Mediated Nucleus Shuttles of Subnanometer Gold Quantum Dots for Real-Time Monitoring of Apoptotic Cell Death. *J. Am. Chem. Soc.* **2010**, *132*, 8309–8315. [CrossRef] [PubMed]

124. Bai, T.T.; Wang, M.; Cao, M.; Zhang, J.; Zhang, K.Z.; Zhou, P.; Liu, Z.X.; Liu, Y.; Guo, Z.R.; Lu, X. Functionalized Au@Ag-Au nanoparticles as an optical and SERS dual probe for lateral flow sensing. *Anal. Bioanal. Chem.* **2018**, *410*, 2291–2303. [CrossRef] [PubMed]

125. He, S.; Kyaw, Y.M.E.; Tan, E.K.M.; Bekale, L.; Kang, M.W.C.; Kim, S.S.Y.; Tan, I.; Lam, K.P.; Kah, J.C.Y. Quantitative and Label-Free Detection of Protein Kinase A Activity Based on Surface-Enhanced Raman Spectroscopy with Gold Nanostars. *Anal. Chem.* **2018**, *90*, 6071–6080. [CrossRef] [PubMed]

126. Xu, S.J.; Liu, Y.; Wang, T.H.; Li, J.H. Highly Sensitive Electrogenerated Chemiluminescence Biosensor in Profiling Protein Kinase Activity and Inhibition Using Gold Nanoparticle as Signal Transduction Probes. *Anal. Chem.* **2010**, *82*, 9566–9572. [CrossRef] [PubMed]

127. Khalilzadeh, B.; Charoudeh, H.N.; Shadjou, N.; Mohammad-Rezaei, R.; Omidi, Y.; Velaei, K.; Aliyari, Z.; Rashidi, M.R. Ultrasensitive caspase-3 activity detection using an electrochemical biosensor engineered by gold nanoparticle functionalized MCM-41: Its application during stem cell differentiation. *Sens. Actuator B Chem.* **2016**, *231*, 561–575. [CrossRef]

128. Parnsubsakul, A.; Safitri, R.E.; Rijiravanich, P.; Surareungchai, W. Electrochemical assay of proteolytically active prostate specific antigen based on anodic stripping voltammetry of silver enhanced gold nanoparticle labels. *J. Electroanal. Chem.* **2017**, *785*, 125–130. [CrossRef]

129. Huang, X.Y.; Liang, Y.R.; Ruan, L.G.; Ren, J.C. Chemiluminescent detection of cell apoptosis enzyme by gold nanoparticle-based resonance energy transfer assay. *Anal. Bioanal. Chem.* **2014**, *406*, 5677–5684. [CrossRef]

130. Hong, Y.; Ku, M.; Lee, E.; Suh, J.S.; Huh, Y.M.; Yoon, D.S.; Yang, J. Localized surface plasmon resonance based nanobiosensor for biomarker detection of invasive cancer cells. *J. Biomed. Opt.* **2014**, *19*, 051202. [CrossRef]

131. Dong, Z.M.; Jin, X.; Zhao, G.C. Amplified QCM biosensor for type IV collagenase based on collagenase-cleavage of gold nanoparticles functionalized peptide. *Biosens. Bioelectron.* **2018**, *106*, 111–116. [CrossRef]

132. Cooper, B.M.; Iegre, J.; O' Donovan, D.H.; Halvarsson, M.O.; Spring, D.R. Peptides as a platform for targeted therapeutics for cancer: Peptide-drug conjugates (PDCs). *Chem. Soc. Rev.* **2021**, *50*, 1480–1494. [CrossRef]

133. Wang, J.; Dai, J.; Yang, X.; Yu, X.Y.; Emory, S.R.; Yong, X.Q.; Xu, J.H.; Mei, L.; Xie, J.B.; Han, N.; et al. Intracellular targeted delivery of quantum dots with extraordinary performance enabled by a novel nanomaterial design. *Nanoscale* **2019**, *11*, 552–567. [CrossRef] [PubMed]

134. Smith, G.P.; Petrenko, V.A. Phage display. *Chem. Rev.* **1997**, *97*, 391–410. [CrossRef] [PubMed]

135. Lam, K.S.; Lebl, M.; Krchnak, V. The "one-bead-one-compound" combinatorial library method. *Chem. Rev.* **1997**, *97*, 411–448. [CrossRef] [PubMed]

136. Wang, Z.H.; Wang, W.Z.; Bu, X.L.; Wei, Z.W.; Geng, L.L.; Wu, Y.; Dong, C.Y.; Li, L.Q.; Zhang, D.; Yang, S.; et al. Microarray Based Screening of Peptide Nano Probes for HER2 Positive Tumor. *Anal. Chem.* **2015**, *87*, 8367–8372. [CrossRef] [PubMed]

137. Lindgren, M.; Hallbrink, M.; Prochiantz, A.; Langel, U. Cell-penetrating peptides. *Trends Pharmacol. Sci.* **2000**, *21*, 99–103. [CrossRef]

138. Josephson, L.; Tung, C.H.; Moore, A.; Weissleder, R. High-efficiency intracellular magnetic labeling with novel superparamagnetic-tat peptide conjugates. *Bioconjugate Chem.* **1999**, *10*, 186–191. [CrossRef]

139. Wunderbaldinger, P.; Josephson, L.; Weissleder, R. Tat peptide directs enhanced clearance and hepatic permeability of magnetic nanoparticles. *Bioconjugate Chem.* **2002**, *13*, 264–268. [CrossRef] [PubMed]

140. Zhao, M.; Kircher, M.F.; Josephson, L.; Weissleder, R. Differential conjugation of tat peptide to superparamagnetic nanoparticles and its effect on cellular uptake. *Bioconjugate Chem.* **2002**, *13*, 840–844. [CrossRef]

141. De la Fuente, J.M.; Berry, C.C. Tat peptide as an efficient molecule to translocate gold nanoparticles into the cell nucleus. *Bioconjugate Chem.* **2005**, *16*, 1176–1180. [CrossRef]

142. Ruan, G.; Agrawal, A.; Marcus, A.I.; Nie, S. Imaging and tracking of tat peptide-conjugated quantum dots in living cells: New insights into nanoparticle uptake, intracellular transport, and vesicle shedding. *J. Am. Chem. Soc.* **2007**, *129*, 14759–14766. [CrossRef] [PubMed]

143. Sun, L.L.; Liu, D.J.; Wang, Z.X. Functional gold nanoparticle-peptide complexes as cell-targeting agents. *Langmuir* **2008**, *24*, 10293–10297. [CrossRef] [PubMed]

144. Sun, L.L.; Wang, J.E.; Wang, Z.X. Recognition and transmembrane delivery of bioconjugated Fe_2O_3@Au nanoparticles with living cells. *Nanoscale* **2010**, *2*, 269–276. [CrossRef] [PubMed]

145. Wei, L.; Yang, Q.Y.; Xiao, L.H. Tempo-spatially resolved cellular dynamics of human immunodeficiency virus transacting activator of transcription (Tat) peptide-modified nanocargos in living cells. *Nanoscale* **2014**, *6*, 10207–10215. [CrossRef]

146. Kostiv, U.; Kotelnikov, I.; Proks, V.; Slouf, M.; Kucka, J.; Engstova, H.; Jezek, P.; Horak, D. RGDS- and TAT-Conjugated Upconversion of $NaYF_4$:Yb^{3+}/Er^{3+} & SiO_2 Nanoparticles: In Vitro Human Epithelioid Cervix Carcinoma Cellular Uptake, Imaging, and Targeting. *ACS Appl. Mater. Interfaces* **2016**, *8*, 20422–20431. [CrossRef]

147. Dalal, C.; Jana, N.R. Multivalency Effect of TAT-Peptide-Functionalized Nanoparticle in Cellular Endocytosis and Subcellular Trafficking. *J. Phys. Chem. B* **2017**, *121*, 2942–2951. [CrossRef]

148. Yong, X.Q.; Yang, X.; Emory, S.R.; Wang, J.; Dai, J.; Yu, X.Y.; Mei, L.; Xie, J.B.; Ruan, G. A potent, minimally invasive and simple strategy of enhancing intracellular targeted delivery of Tat peptide-conjugated quantum dots: Organic solvent-based permeation enhancer. *Biomater. Sci.* **2018**, *6*, 3085–3095. [CrossRef]

149. Chen, L.J.; Zhao, X.; Yan, X.P. Cell-Penetrating Peptide-Functionalized Persistent Luminescence Nanoparticles for Tracking J774A.1 Macrophages Homing to Inflamed Tissues. *ACS Appl. Mater. Interfaces* **2019**, *11*, 19894–19901. [CrossRef]

150. Shukla, R.; Hill, E.; Shi, X.Y.; Kim, J.; Muniz, M.C.; Sun, K.; Baker, J.R. Tumor microvasculature targeting with dendrimer-entrapped gold nanoparticles. *Soft Matter* **2008**, *4*, 2160–2163. [CrossRef]

151. Li, K.; Zhang, Z.P.; Luo, M.; Yu, X.; Han, Y.; Wei, H.P.; Cui, Z.Q.; Zhang, X.E. Multifunctional ferritin cage nanostructures for fluorescence and MR imaging of tumor cells. *Nanoscale* **2012**, *4*, 188–193. [CrossRef]

152. Lu, Y.M.; Zhong, Y.L.; Wang, J.; Su, Y.Y.; Peng, F.; Zhou, Y.F.; Jiang, X.X.; He, Y. Aqueous synthesized near-infrared-emitting quantum dots for RGD-based in vivo active tumour targeting. *Nanotechnology* **2013**, *24*, 135101. [CrossRef]

153. Cheng, K.; Kothapalli, S.R.; Liu, H.G.; Koh, A.L.; Jokerst, J.V.; Jiang, H.; Yang, M.; Li, J.B.; Levi, J.; Wu, J.C.; et al. Construction and Validation of Nano Gold Tripods for Molecular Imaging of Living Subjects. *J. Am. Chem. Soc.* **2014**, *136*, 3560–3571. [CrossRef]

154. Yan, J.; He, W.X.; Li, N.; Yu, M.; Du, Y.P.; Lei, B.; Ma, P.X. Simultaneously targeted imaging cytoplasm and nucleus in living cell by biomolecules capped ultra-small GdOF nanocrystals. *Biomaterials* **2015**, *59*, 21–29. [CrossRef] [PubMed]

155. Tang, R.; Xue, J.P.; Xu, B.G.; Shen, D.W.; Sudlow, G.P.; Achilefu, S. Tunable Ultrasmall Visible-to-Extended Near-Infrared Emitting Silver Sulfide Quantum Dots for Integrin-Targeted Cancer Imaging. *ACS Nano* **2015**, *9*, 220–230. [CrossRef] [PubMed]

156. Chen, Q.; Wang, H.; Liu, H.; Wen, S.H.; Peng, C.; Shen, M.W.; Zhang, G.X.; Shi, X.Y. Multifunctional Dendrimer-Entrapped Gold Nanoparticles Modified with RGD Peptide for Targeted Computed Tomography/Magnetic Resonance Dug-Modal Imaging of Tumors. *Anal. Chem.* **2015**, *87*, 3949–3956. [CrossRef] [PubMed]

157. Yang, J.; Luo, Y.; Xu, Y.H.; Li, J.C.; Zhang, Z.X.; Wang, H.; Shen, M.W.; Shi, X.Y.; Zhang, G.X. Conjugation of Iron Oxide Nanoparticles with RGD-Modified Dendrimers for Targeted Tumor MR Imaging. *ACS Appl. Mater. Interfaces* **2015**, *7*, 5420–5428. [CrossRef]

158. Meng, F.Y.; Han, K.; Wang, B.D.; Liu, T.; Liu, G.X.; Li, Y.R.; Miao, P. Nanoarchitectured Electrochemical Cytosensor for Selective Detection of Cancer Cells. *Chemistryselect* **2016**, *1*, 1515–1517. [CrossRef]

159. Meidell, K.Z.; Robinson, R.; Vieira-de-Abreu, A.; Gormley, A.J.; Ghandehari, H.; Grainger, D.W.; Campbell, R.A. RGDfK-functionalized gold nanorods bind only to activated platelets. *J. Biomed. Mater. Res. A* **2017**, *105*, 209–217. [CrossRef]

160. Boucher, M.; Geffroy, F.; Preveral, S.; Bellanger, L.; Selingue, E.; Adryanczyk-Perrier, G.; Pean, M.; Lefevre, C.T.; Pignol, D.; Ginet, N.; et al. Genetically tailored magnetosomes used as MRI probe for molecular imaging of brain tumor. *Biomaterials* **2017**, *121*, 167–178. [CrossRef]

161. Su, G.X.; Jiang, H.Q.; Xu, B.H.; Yu, Y.Y.; Chen, X.Q. Effects of Protein Corona on Active and Passive Targeting of Cyclic RGD Peptide-Functionalized PEGylation Nanoparticles. *Mol. Pharmaceutics* **2018**, *15*, 5019–5030. [CrossRef]

162. Simitzi, C.; Harimech, P.; Spanou, S.; Lanara, C.; Heuer-Jungemann, A.; Manousaki, A.; Fotakis, C.; Ranella, A.; Kanaras, A.G.; Stratakis, E. Cells on hierarchically-structured platforms hosting functionalized nanoparticles. *Biomater. Sci.* **2018**, *6*, 1469–1479. [CrossRef] [PubMed]

163. Yin, X.H.; Li, X.L.; Zhu, C.L.; Lin, X.C.; Xie, Z.H. Integration of fluorescence/photoacoustic imaging and targeted chemo/photothermal therapy with Ag$_2$Se@BSA-RGD nanodots. *New J. Chem.* **2020**, *44*, 4850–4857. [CrossRef]

164. Gao, H.Y.; Chu, C.C.; Cheng, Y.; Zhang, Y.; Pang, X.; Li, D.F.; Wang, X.Y.; Ren, E.; Xie, F.F.; Bai, Y.; et al. In Situ Formation of Nanotheranostics to Overcome the Blood-Brain Barrier and Enhance Treatment of Orthotopic Glioma. *ACS Appl. Mater. Interfaces* **2020**, *12*, 26880–26892. [CrossRef] [PubMed]

165. Bunschoten, A.; Chin, P.T.K.; Buckle, T.; van der Linden, M.; Barendregt, A.; Verheijen, M.A.; van Leeuwen, F.W.B. Receptor-Targeted Luminescent Silver Bionanoparticles. *Eur. J. Inorg. Chem.* **2016**, 3030–3035. [CrossRef]

166. Willmore, A.M.A.; Simon-Gracia, L.; Toome, K.; Paiste, P.; Kotamraju, V.R.; Molder, T.; Sugahara, K.N.; Ruoslahti, E.; Braun, G.B.; Teesalu, T. Targeted silver nanoparticles for ratiometric cell phenotyping. *Nanoscale* **2016**, *8*, 9096–9101. [CrossRef] [PubMed]

167. Goncalves, D.P.N.; Rodriguez, R.D.; Kurth, T.; Bray, L.J.; Binner, M.; Jungnickel, C.; Gur, F.N.; Poser, S.W.; Schmidt, T.L.; Zahn, D.R.T.; et al. Enhanced targeting of invasive glioblastoma cells by peptide-functionalized gold nanorods in hydrogel-based 3D cultures. *Acta Biomater.* **2017**, *58*, 12–25. [CrossRef]

168. Toome, K.; Willmore, A.M.A.; Paiste, P.; Tobi, A.; Sugahara, K.N.; Kirsimae, K.; Ruoslahti, E.; Braun, G.B.; Teesalu, T. Ratiometric in vivo auditioning of targeted silver nanoparticles. *Nanoscale* **2017**, *9*, 10094–10100. [CrossRef] [PubMed]

169. Liu, G.F.; Chen, H.D.; Yu, S.N.; Li, X.D.; Wang, Z.X. CXCR4 Peptide Conjugated Au-Fe2O3 Nanoparticles for Tumor-targeting Magnetic Resonance Imaging. *Chem. Res. Chin. Univ.* **2018**, *34*, 584–589. [CrossRef]

170. Goncalves, D.P.N.; Park, D.M.; Schmidt, T.L.; Werner, C. Modular peptide-functionalized gold nanorods for effective glioblastoma multicellular tumor spheroid targeting. *Biomater. Sci.* **2018**, *6*, 1140–1146. [CrossRef]

171. Lingasamy, P.; Tobi, A.; Haugas, M.; Hunt, H.; Paiste, P.; Asser, T.; Ratsep, T.; Kotamraju, V.R.; Bjerkvig, R.; Teesalu, T. Bi-specific tenascin-C and fibronectin targeted peptide for solid tumor delivery. *Biomaterials* **2019**, *219*, 119373. [CrossRef]

172. Zhao, L.Z.; Li, Y.J.; Zhu, J.Y.; Sun, N.; Song, N.N.; Xing, Y.; Huang, H.; Zhao, J.H. Chlorotoxin peptide-functionalized polyethylenimine-entrapped gold nanoparticles for glioma SPECT/CT imaging and radionuclide therapy. *J. Nanobiotechnol.* **2019**, *17*, 30. [CrossRef] [PubMed]

173. Lee, T.Y.; Lin, C.T.; Kuo, S.Y.; Chang, D.K.; Wu, H.C. Peptide-mediated targeting to tumor blood vessels of lung cancer for drug delivery. *Cancer Res.* **2007**, *67*, 10958–10965. [CrossRef] [PubMed]

174. Potente, M.; Gerhardt, H.; Carmeliet, P. Basic and Therapeutic Aspects of Angiogenesis. *Cell* **2011**, *146*, 873–887. [CrossRef]

175. Weis, S.M.; Cheresh, D.A. Tumor angiogenesis: Molecular pathways and therapeutic targets. *Nat. Med.* **2011**, *17*, 1359–1370. [CrossRef]

176. De Palma, M.; Biziato, D.; Petrova, T.V. Microenvironmental regulation of tumour angiogenesis. *Nat. Rev. Cancer* **2017**, *17*, 457–474. [CrossRef]

177. Fu, X.Y.; Yang, Y.H.; Li, X.L.; Lai, H.Q.; Huang, Y.Y.; He, L.Z.; Zheng, W.J.; Chen, T.F. RGD peptide-conjugated selenium nanoparticles: Antiangiogenesis by suppressing VEGF-VEGFR2-ERK/AKT pathway. *Nanomed. Nanotechnol.* **2016**, *12*, 1627–1639. [CrossRef]

178. Hu, H.; You, Y.Y.; He, L.Z.; Chen, T.F. The rational design of NAMI-A-loaded mesoporous silica nanoparticles as antiangiogenic nanosystems. *J. Mater. Chem. B* **2015**, *3*, 6338–6346. [CrossRef] [PubMed]

179. Tang, M.M.; Ji, X.Y.; Xu, H.; Zhang, L.; Jiang, A.R.; Song, B.; Su, Y.Y.; He, Y. Photostable and Biocompatible Fluorescent Silicon Nanoparticles-Based Theranostic Probes for Simultaneous Imaging and Treatment of Ocular Neovascularization. *Anal. Chem.* **2018**, *90*, 8188–8195. [CrossRef] [PubMed]

180. Wang, Y.F.; Tong, L.; Wang, J.G.; Luo, J.M.; Tang, J.; Zhong, L.J.; Xiao, Q.; Niu, W.B.; Li, J.H.; Zhu, J.Q.; et al. cRGD-functionalized nanoparticles for combination therapy of anti-endothelium dependent vessels and anti-vasculogenic mimicry to inhibit the proliferation of ovarian cancer. *Acta Biomater.* **2019**, *94*, 495–504. [CrossRef]

181. Li, Q.R.; Zhou, R.H.; Sun, Y.; Xiao, D.X.; Liu, M.T.; Zhao, D.; Peng, S.L.; Chen, Y.; Lin, Y.F. Synthesis and Antitumor Application of Antiangiogenetic Gold Nanoclusters. *ACS Appl. Mater. Interfaces* **2021**, *13*, 11708–11720. [CrossRef]

182. Abadeer, N.S.; Murphy, C.J. Recent Progress in Cancer Thermal Therapy Using Gold Nanoparticles. *J. Phys. Chem. C* **2016**, *120*, 4691–4716. [CrossRef]

183. Liu, Y.; Ji, M.; Wang, P. Recent Advances in Small Copper Sulfide Nanoparticles for Molecular Imaging and Tumor Therapy. *Mol. Pharm.* **2019**, *16*, 3322–3332. [CrossRef]

184. Seaberg, J.; Montazerian, H.; Hossen, M.N.; Bhattacharya, R.; Khademhosseini, A.; Mukherjee, P. Hybrid Nanosystems for Biomedical Applications. *ACS Nano* **2021**, *15*, 2099–2142. [CrossRef] [PubMed]

185. Yuan, H.; Fales, A.M.; Vo-Dinh, T. TAT Peptide-Functionalized Gold Nanostars: Enhanced Intracellular Delivery and Efficient NIR Photothermal Therapy Using Ultralow Irradiance. *J. Am. Chem. Soc.* **2012**, *134*, 11358–11361. [CrossRef] [PubMed]

186. Lee, U.Y.; Youn, Y.S.; Park, J.; Lee, E.S. Y-Shaped Ligand-Driven Gold Nanoparticles for Highly Efficient Tumoral Uptake and Photothermal Ablation. *ACS Nano* **2014**, *8*, 12858–12865. [CrossRef] [PubMed]

187. Ali, M.R.K.; Wu, Y.; Tang, Y.; Xiao, H.P.; Chen, K.C.; Han, T.G.; Fang, N.; Wu, R.H.; El-Sayed, M.A. Targeting cancer cell integrins using gold nanorods in photothermal therapy inhibits migration through affecting cytoskeletal proteins. *Proc. Natl Acad. Sci. USA* **2017**, *114*, E5655–E5663. [CrossRef]

188. Peng, H.B.; Tang, J.; Zheng, R.; Guo, G.N.; Dong, A.G.; Wang, Y.J.; Yang, W.L. Nuclear-Targeted Multifunctional Magnetic Nanoparticles for Photothermal Therapy. *Adv. Healthc. Mater.* **2017**, *6*, 1601289. [CrossRef]

189. Li, N.; Sun, Q.Q.; Yu, Z.Z.; Gao, X.N.; Pan, W.; Wan, X.Y.; Tang, B. Nuclear-Targeted Photothermal Therapy Prevents Cancer Recurrence with Near-Infrared Triggered Copper Sulfide Nanoparticles. *ACS Nano* **2018**, *12*, 5197–5206. [CrossRef]

190. Arriortua, O.K.; Insausti, M.; Lezama, L.; de Muro, I.G.; Garaio, E.; de la Fuente, J.M.; Fratila, R.M.; Morales, M.P.; Costa, R.; Eceiza, M.; et al. RGD-Functionalized Fe$_3$O$_4$ nanoparticles for magnetic hyperthermia. *Colloid Surf. B* **2018**, *165*, 315–324. [CrossRef]

191. Zong, J.Y.; Cobb, S.L.; Cameron, N.R. Short elastin- like peptide- functionalized gold nanoparticles that are temperature responsive under near- physiological conditions. *J. Mater. Chem. B* **2018**, *6*, 6667–6674. [CrossRef]

192. Liao, Y.T.; Liu, C.H.; Chin, Y.; Chen, S.Y.; Liu, S.H.; Hsu, Y.C.; Wu, K.C.W. Biocompatible and multifunctional gold nanorods for effective photothermal therapy of oral squamous cell carcinoma. *J. Mater. Chem. B* **2019**, *7*, 4451–4460. [CrossRef]

193. Huang, X.; Yin, Y.L.; Wu, M.; Zan, W.; Yang, Q. LyP-1 peptide-functionalized gold nanoprisms for SERRS imaging and tumor growth suppressing by PTT induced-hyperthermia. *Chin. Chem. Lett.* **2019**, *30*, 1335–1340. [CrossRef]

194. Li, B.; Zhou, Q.; Wang, H.Y.; Zha, Y.C.; Zheng, P.L.; Yang, T.; Ma, D.; Qiu, L.; Xu, X.M.; Hu, Y.; et al. Mitochondria-targeted magnetic gold nanoheterostructure for multi-modal imaging guided photothermal and photodynamic therapy of triple-negative breast cancer. *Chem. Eng. J.* **2021**, *403*, 126364. [CrossRef]

195. Qiu, L.P.; Valente, M.; Dolen, Y.; Jager, E.; ter Beest, M.; Zheng, L.Y.; Figdor, C.G.; Verdoes, M. Endolysosomal-Escape Nanovaccines through Adjuvant-Induced Tumor Antigen Assembly for Enhanced Effector CD8(+) T Cell Activation. *Small* **2018**, *14*, 1703539. [CrossRef] [PubMed]

196. Cruje, C.; Yang, C.; Uertz, J.; van Prooijen, M.; Chithrani, B.D. Optimization of PEG coated nanoscale gold particles for enhanced radiation therapy. *RSC Adv.* **2015**, *5*, 101525–101532. [CrossRef]

197. Zhao, N.; Yang, Z.R.; Li, B.X.; Meng, J.; Shi, Z.L.; Li, P.; Fu, S. RGD-conjugated mesoporous silica-encapsulated gold nanorods enhance the sensitization of triple-negative breast cancer to megavoltage radiation therapy. *Int. J. Nanomed.* **2016**, *11*, 5595–5610. [CrossRef] [PubMed]

198. Chilug, L.E.; Leonte, R.A.; Barbinta Patrascu, M.E.; Ion, A.C.; Tuta, C.S.; Raicu, A.; Manda, G.; Niculae, D. In vitro binding kinetics study of gold nanoparticles functionalized with Ga-68-DOTA conjugated peptides. *J. Radioanal. Nucl. Chem.* **2017**, *311*, 1485–1493. [CrossRef]

199. Chakravarty, R.; Chakraborty, S.; Guleria, A.; Kumar, C.; Kunwar, A.; Nair, K.V.V.; Sarma, H.D.; Dash, A. Clinical scale synthesis of intrinsically radiolabeled and cyclic RGD peptide functionalized Au-198 nanoparticles for targeted cancer therapy. *Nucl. Med. Biol.* **2019**, *72–73*, 1–10. [CrossRef] [PubMed]

200. Hafsi, M.; Preveral, S.; Hoog, C.; Herault, J.; Perrier, G.A.; Lefevre, C.T.; Michel, H.; Pignol, D.; Doyen, J.; Pourcher, T.; et al. RGD-functionalized magnetosomes are efficient tumor radioenhancers for X-rays and protons. *Nanomed. Nanotechnol.* **2020**, *23*, 102084. [CrossRef]

201. Zhang, J.; Yuan, Z.F.; Wang, Y.; Chen, W.H.; Luo, G.F.; Cheng, S.X.; Zhuo, R.X.; Zhang, X.Z. Multifunctional Envelope-Type Mesoporous Silica Nanoparticles for Tumor-Triggered Targeting Drug Delivery. *J. Am. Chem. Soc.* **2013**, *135*, 5068–5073. [CrossRef]

202. Black, K.C.L.; Akers, W.J.; Sudlow, G.; Xu, B.G.; Laforest, R.; Achilefu, S. Dual-radiolabeled nanoparticle SPECT probes for bioimaging. *Nanoscale* **2015**, *7*, 440–444. [CrossRef]

203. Zhao, X.; Yang, C.X.; Chen, L.G.; Yan, X.P. Dual-stimuli responsive and reversibly activatable theranostic nanoprobe for precision tumor-targeting and fluorescence-guided photothermal therapy. *Nat. Commun.* **2017**, *8*, 14998. [CrossRef]

204. Ma, T.C.; Hou, Y.; Zeng, J.F.; Liu, C.Y.; Zhang, P.S.; Jing, L.H.; Shangguan, D.; Gao, M.Y. Dual-Ratiometric Target-Triggered Fluorescent Probe for Simultaneous Quantitative Visualization of Tumor Microenvironment Protease Activity and pH &ITin Vivo&IT. *J. Am. Chem. Soc.* **2018**, *140*, 211–218. [CrossRef]

205. Han, H.J.; Hou, Y.; Chen, X.H.; Zhang, P.S.; Kang, M.X.; Jin, Q.; Ji, J.; Gao, M.Y. Metformin-Induced Stromal Depletion to Enhance the Penetration of Gemcitabine-Loaded Magnetic Nanoparticles for Pancreatic Cancer Targeted Therapy. *J. Am. Chem. Soc.* **2020**, *142*, 4944–4954. [CrossRef]

206. Zha, S.; Chau, H.F.; Chau, W.Y.; Chan, L.S.; Lin, J.; Lo, K.W.; Cho, W.C.S.; Yip, Y.L.; Tsao, S.W.; Farrell, P.J.; et al. Dual-Targeting Peptide-Guided Approach for Precision Delivery and Cancer Monitoring by Using a Safe Upconversion Nanoplatform. *Adv. Sci.* **2021**, *8*, 2002919. [CrossRef] [PubMed]

207. Lin, B.; Wu, J.; Wang, Y.X.; Sun, S.; Yuan, Y.; Tao, X.F.; Lv, R.C. Peptide functionalized upconversion/NIR II luminescent nanoparticles for targeted imaging and therapy of oral squamous cell carcinoma. *Biomater. Sci.* **2021**, *9*, 1000–1007. [CrossRef] [PubMed]

208. Yang, X.Q.; Hong, H.; Grailer, J.J.; Rowland, I.J.; Javadi, A.; Hurley, S.A.; Xiao, Y.L.; Yang, Y.A.; Zhang, Y.; Nickles, R.; et al. cRGD-functionalized, DOX-conjugated, and Cu-64-labeled superparamagnetic iron oxide nanoparticles for targeted anticancer drug delivery and PET/MR imaging. *Biomaterials* **2011**, *32*, 4151–4160. [CrossRef] [PubMed]

209. Lee, J.; Lee, T.S.; Ryu, J.; Hong, S.; Kang, M.; Im, K.; Kang, J.H.; Lim, S.M.; Park, S.; Song, R. RGD Peptide-Conjugated Multimodal NaGdF$_4$:Yb^{3+}/Er^{3+} Nanophosphors for Upconversion Luminescence, MR, and PET Imaging of Tumor Angiogenesis. *J. Nucl. Med.* **2013**, *54*, 96–103. [CrossRef] [PubMed]

210. Cedrowska, E.; Pruszynski, M.; Majkowska-Pilip, A.; Meczynska-Wielgosz, S.; Bruchertseifer, F.; Morgenstern, A.; Bilewicz, A. Functionalized TiO$_2$ nanoparticles labelled with Ac-225 for targeted alpha radionuclide therapy. *J. Nanopart. Res.* **2018**, *20*, 83. [CrossRef] [PubMed]

211. Pan, L.M.; He, Q.J.; Liu, J.N.; Chen, Y.; Ma, M.; Zhang, L.L.; Shi, J.L. Nuclear-Targeted Drug Delivery of TAT Peptide-Conjugated Monodisperse Mesoporous Silica Nanoparticles. *J. Am. Chem. Soc.* **2012**, *134*, 5722–5725. [CrossRef]

212. Luo, G.F.; Chen, W.H.; Liu, Y.; Zhang, J.; Cheng, S.X.; Zhuo, R.X.; Zhang, X.Z. Charge-reversal plug gate nanovalves on peptide-functionalized mesoporous silica nanoparticles for targeted drug delivery. *J. Mater. Chem. B* **2013**, *1*, 5723–5732. [CrossRef]

213. Kinnari, P.J.; Hyvonen, M.L.K.; Makila, E.M.; Kaasalainen, M.H.; Rivinoja, A.; Salonen, J.J.; Hirvonen, J.T.; Laakkonen, P.M.; Santos, H.A. Tumour homing peptide-functionalized porous silicon nanovectors for cancer therapy. *Biomaterials* **2013**, *34*, 9134–9141. [CrossRef]

214. Sun, J.; Kim, D.H.; Guo, Y.; Teng, Z.G.; Li, Y.J.; Zheng, L.F.; Zhang, Z.L.; Larson, A.C.; Lu, G.M. A c(RGDfE) conjugated multi-functional nanomedicine delivery system for targeted pancreatic cancer therapy. *J. Mater. Chem. B* **2015**, *3*, 1049–1058. [CrossRef] [PubMed]

215. Lai, J.P.; Shah, B.R.; Zhang, Y.X.; Yang, L.T.; Lee, K.B. Real-Time Monitoring of ATP-Responsive Drug Release Using Mesoporous-Silica-Coated Multicolor Upconversion Nanoparticles. *ACS Nano* **2015**, *9*, 5234–5245. [CrossRef]

216. Chen, G.C.; Xie, Y.S.; Peltier, R.; Lei, H.P.; Wang, P.; Chen, J.; Hu, Y.; Wang, F.; Yao, X.; Sun, H.Y. Peptide-Decorated Gold Nanoparticles as Functional Nano-Capping Agent of Mesoporous Silica Container for Targeting Drug Delivery. *ACS Appl. Mater. Interfaces* **2016**, *8*, 11204–11209. [CrossRef] [PubMed]

217. Noh, G.; Youn, Y.S.; Lee, E.S. Preparation of iron oxide nanoparticles functionalized with Y-shaped ligands for brain tumor targeting. *J. Mater. Chem. B* **2016**, *4*, 6074–6080. [CrossRef] [PubMed]

218. Chen, W.H.; Luo, G.F.; Lei, Q.; Cao, F.Y.; Fan, J.X.; Qiu, W.X.; Jia, H.Z.; Hong, S.; Fang, F.; Zeng, X.; et al. Rational design of multifunctional magnetic mesoporous silica nanoparticle for tumor-targeted magnetic resonance imaging and precise therapy. *Biomaterials* **2016**, *76*, 87–101. [CrossRef]

219. Zhang, X.M.; Ai, F.J.; Sun, T.Y.; Wang, F.; Zhu, G.Y. Multimodal Upconversion Nanoplatform with a Mitochondria-Targeted Property for Improved Photodynamic Therapy of Cancer Cells. *Inorg. Chem.* **2016**, *55*, 3872–3880. [CrossRef]

220. Han, L.; Tang, C.; Yin, C.H. pH-Responsive Core-Shell Structured Nanoparticles for Triple-Stage Targeted Delivery of Doxorubicin to Tumors. *ACS Appl. Mater. Interfaces* **2016**, *8*, 23498–23508. [CrossRef] [PubMed]

221. Wang, Y.P.; Liao, Y.T.; Liu, C.H.; Yu, J.S.; Alamri, H.R.; Alothman, Z.A.; Hossain, M.S.A.; Yamauchi, Y.; Wu, K.C.W. Trifunctional Fe$_3$O$_4$/CaP/Alginate Core-Shell-Corona Nanoparticles for Magnetically Guided, pH-Responsive, and Chemically Targeted Chemotherapy. *ACS Biomater. Sci. Eng.* **2017**, *3*, 2366–2374. [CrossRef]

222. Wu, J.L.; He, X.Y.; Liu, B.Y.; Gong, M.Q.; Zhuo, R.X.; Cheng, S.X. Fusion peptide functionalized hybrid nanoparticles for synergistic drug delivery to reverse cancer drug resistance. *J. Mater. Chem. B* **2017**, *5*, 4697–4704. [CrossRef]

223. Chan, M.S.; Liu, L.S.; Leung, H.M.; Lo, P.K. Cancer-Cell-Specific Mitochondria-Targeted Drug Delivery by Dual-Ligand-Functionalized Nanodiamonds Circumvent Drug Resistance. *ACS Appl. Mater. Interfaces* **2017**, *9*, 11780–11789. [CrossRef] [PubMed]

224. Huang, S.N.; Li, C.M.; Wang, W.P.; Li, H.J.; Sun, Z.; Song, C.Z.; Li, B.Y.; Duan, S.F.; Hu, Y.R. A 54 peptide-mediated functionalized gold nanocages for targeted delivery of DOX as a combinational photothermal-chemotherapy for liver cancer. *Int. J. Nanomed.* **2017**, *12*, 5163–5176. [CrossRef] [PubMed]

225. Sun, X.; Luo, Y.P.; Huang, L.W.; Yu, B.Y.; Tian, J.W. A peptide-decorated and curcumin-loaded mesoporous silica nanomedicine for effectively overcoming multidrug resistance in cancer cells. *RSC Adv.* **2017**, *7*, 16401–16409. [CrossRef]

226. Xia, Y.; Chen, Y.; Hua, L.; Zhao, M.Q.; Xu, T.T.; Wang, C.B.; Li, Y.H.; Zhu, B. Functionalized selenium nanoparticles for targeted delivery of doxorubicin to improve non-small-cell lung cancer therapy. *Int. J. Nanomed.* **2018**, *13*, 6929–6939. [CrossRef]

227. Dalmau-Mena, I.; del Pino, P.; Pelaz, B.; Cuesta-Geijo, M.A.; Galindo, I.; Moros, M.; de la Fuente, J.M.; Alonso, C. Nanoparticles engineered to bind cellular motors for efficient delivery. *J. Nanobiotechnol.* **2018**, *16*, 33. [CrossRef]

228. Ai, F.J.; Wang, N.; Zhang, X.M.; Sun, T.Y.; Zhu, Q.; Kong, W.; Wang, F.; Zhu, G.Y. An upconversion nanoplatform with extracellular pH-driven tumor-targeting ability for improved photodynamic therapy. *Nanoscale* **2018**, *10*, 4432–4441. [CrossRef]

229. Xiao, Z.Y.; Chan, L.; Zhang, D.; Huang, C.Q.; Mei, C.M.; Gao, P.; Huang, Y.Y.; Liang, J.Y.; He, L.Z.; Shi, C.Z.; et al. Precise delivery of a multifunctional nanosystem for MRI-guided cancer therapy and monitoring of tumor response by functional diffusion-weighted MRI. *J. Mater. Chem. B* **2019**, *7*, 2926–2937. [CrossRef]

230. Ruan, L.P.; Chen, W.; Wang, R.N.; Lu, J.; Zink, J.I. Magnetically Stimulated Drug Release Using Nanoparticles Capped by Self-Assembling Peptides. *ACS Appl. Mater. Interfaces* **2019**, *11*, 43835–43842. [CrossRef]

231. Hou, L.; Chen, D.D.; Wang, R.T.; Wang, R.B.; Zhang, H.J.; Zhang, Z.Z.; Nie, Z.H.; Lu, S.Y. Transformable Honeycomb-Like Nanoassemblies of Carbon Dots for Regulated Multisite Delivery and Enhanced Antitumor Chemoimmunotherapy. *Angew. Chem. Int. Ed.* **2021**, *60*, 6581–6592. [CrossRef] [PubMed]

232. Burnett, J.C.; Rossi, J.J. RNA-Based Therapeutics: Current Progress and Future Prospects. *Chem. Biol.* **2012**, *19*, 60–71. [CrossRef]

233. Jung, J.J.; Solanki, A.; Memoli, K.A.; Kamei, K.; Kim, H.; Drahl, M.A.; Williams, L.J.; Tseng, H.R.; Lee, K. Selective Inhibition of Human Brain Tumor Cells through Multifunctional Quantum-Dot-Based siRNA Delivery. *Angew. Chem. Int. Ed.* **2010**, *49*, 103–107. [CrossRef] [PubMed]

234. Veiseh, O.; Kievit, F.M.; Fang, C.; Mu, N.; Jana, S.; Leung, M.C.; Mok, H.; Ellenbogen, R.G.; Park, J.O.; Zhang, M.Q. Chlorotoxin bound magnetic nanovector tailored for cancer cell targeting, imaging, and siRNA delivery. *Biomaterials* **2010**, *31*, 8032–8042. [CrossRef] [PubMed]

235. Li, J.M.; Wang, Y.Y.; Zhao, M.X.; Tan, C.P.; Li, Y.Q.; Le, X.Y.; Ji, L.N.; Mao, Z.W. Multifunctional QD-based co-delivery of siRNA and doxorubicin to HeLa cells for reversal of multidrug resistance and real-time tracking. *Biomaterials* **2012**, *33*, 2780–2790. [CrossRef] [PubMed]

236. Li, X.; Chen, Y.J.; Wang, M.Q.; Ma, Y.J.; Xia, W.L.; Gu, H.C. A mesoporous silica nanoparticle—PEI—Fusogenic peptide system for siRNA delivery in cancer therapy. *Biomaterials* **2013**, *34*, 1391–1401. [CrossRef] [PubMed]

237. Chen, Y.J.; Gu, H.C.; Zhang, D.S.Z.; Li, F.; Liu, T.Y.; Xia, W.L. Highly effective inhibition of lung cancer growth and metastasis by systemic delivery of siRNA via multimodal mesoporous silica-based nanocarrier. *Biomaterials* **2014**, *35*, 10058–10069. [CrossRef]

238. Wang, F.H.; Zhang, W.J.; Shen, Y.Y.; Huang, Q.; Zhou, D.J.; Guo, S.R. Efficient RNA delivery by integrin-targeted glutathione responsive polyethyleneimine capped gold nanorods. *Acta Biomater.* **2015**, *23*, 136–146. [CrossRef] [PubMed]

239. Xia, Y.; Lin, Z.F.; Li, Y.H.; Zhao, M.Q.; Wang, C.B.; Guo, M.; Zhang, B.; Zhu, B. Targeted delivery of siRNA using RGDfC-conjugated functionalized selenium nanoparticles for anticancer therapy. *J. Mater. Chem. B* **2017**, *5*, 6941–6952. [CrossRef]

240. Xia, Y.; Xu, T.T.; Wang, C.B.; Li, Y.H.; Lin, Z.F.; Zhao, M.Q.; Zhu, B. Novel functionalized nanoparticles for tumor-targeting co-delivery of doxorubicin and siRNA to enhance cancer therapy. *Int. J. Nanomed.* **2018**, *13*, 143–159. [CrossRef]

241. Xia, Y.; Tang, G.Y.; Wang, C.B.; Zhong, J.Y.; Chen, Y.; Hua, L.; Li, Y.H.; Liu, H.S.; Zhu, B. Functionalized selenium nanoparticles for targeted siRNA delivery silence Derlin1 and promote antitumor efficacy against cervical cancer. *Drug Deliv.* **2020**, *27*, 15–25. [CrossRef]

242. Wang, C.B.; Xia, Y.; Huo, S.C.; Shou, D.W.; Mei, Q.; Tang, W.J.; Li, Y.H.; Liu, H.S.; Zhou, Y.J.; Zhu, B. Silencing of MEF2D by siRNA Loaded Selenium Nanoparticles for Ovarian Cancer Therapy. *Int. J. Nanomed.* **2020**, *15*, 9759–9770. [CrossRef] [PubMed]

243. Xia, Y.; Tang, G.Y.; Guo, M.; Xu, T.T.; Chen, H.Y.; Lin, Z.F.; Li, Y.H.; Chen, Y.; Zhu, B.; Liu, H.S.; et al. Silencing KLK12 expression via RGDfC-decorated selenium nanoparticles for the treatment of colorectal cancer in vitro and in vivo. *Mat. Sci. Eng. C Mater.* **2020**, *110*, 110594. [CrossRef] [PubMed]

244. Ben Djemaa, S.; David, S.; Herve-Aubert, K.; Falanga, A.; Galdiero, S.; Allard-Vannier, E.; Chourpa, I.; Munnier, E. Formulation and in vitro evaluation of a siRNA delivery nanosystem decorated with gH625 peptide for triple negative breast cancer theranosis. *Eur. J. Pharm. Biopharm.* **2018**, *131*, 99–108. [CrossRef] [PubMed]

245. Ben Djemaa, S.; Herve-Aubert, K.; Lajoie, L.; Falanga, A.; Galdiero, S.; Nedellec, S.; Souce, M.; Munnier, E.; Chourpa, I.; David, S.; et al. gH625 Cell-Penetrating Peptide Promotes the Endosomal Escape of Nanovectorized siRNA in a Triple-Negative Breast Cancer Cell Line. *Biomacromolecules* **2019**, *20*, 3076–3086. [CrossRef] [PubMed]

246. Leung, H.M.; Chan, M.S.; Liu, L.S.; Wong, S.W.; Lo, T.W.; Lau, C.H.; Tin, C.; Lo, P.K. Dual-Function, Cationic, Peptide-Coated Nanodiamond Systems: Facilitating Nuclear-Targeting Delivery for Enhanced Gene Therapy Applications. *ACS Sustain. Chem. Eng.* **2018**, *6*, 9671–9681. [CrossRef]

247. Zhang, Y.; Song, G.B.; He, Y.L.; Zhang, X.B.; Liu, Y.; Ju, H.X. A DNA-Azobenzene Nanopump Fueled by Upconversion Luminescence for Controllable Intracellular Drug Release. *Angew. Chem. Int. Ed.* **2019**, *58*, 18207–18211. [CrossRef] [PubMed]

248. Huang, H.Q.; Yuan, S.R.; Ma, Z.; Ji, P.; Ma, X.N.; Wu, Z.H.; Qi, X.L. Genetic recombination of poly(l-lysine) functionalized apoferritin nanocages that resemble viral capsid nanometer-sized platforms for gene therapy. *Biomater. Sci.* **2020**, *8*, 1759–1770. [CrossRef]

249. Veiseh, O.; Kievit, F.M.; Liu, V.; Fang, C.; Stephen, Z.R.; Ellenbogen, R.G.; Zhang, M.Q. In Vivo Safety Evaluation of Polyarginine Coated Magnetic Nanovectors. *Mol. Pharm.* **2013**, *10*, 4099–4106. [CrossRef]

250. Sarkar, K.; Banerjee, S.L.; Kundu, P.P.; Madras, G.; Chatterjee, K. Biofunctionalized surface-modified silver nanoparticles for gene delivery. *J. Mater. Chem. B* **2015**, *3*, 5266–5276. [CrossRef]

251. Chen, Y.J.; Wang, X.R.; Liu, T.; Zhang, D.S.Z.; Wang, Y.F.; Gu, H.C.; Di, W. Highly effective antiangiogenesis via magnetic mesoporous silica-based siRNA vehicle targeting the VEGF gene for orthotopic ovarian cancer therapy. *Int. J. Nanomed.* **2015**, *10*, 2579–2594. [CrossRef]

252. Kong, L.D.; Qiu, J.R.; Shi, X.Y. Multifunctional PEI-entrapped gold nanoparticles enable efficient delivery of therapeutic siRNA into glioblastoma cells. *J. Control. Release* **2017**, *259*, E83–E84. [CrossRef]

253. Li, N.; Yang, H.J.; Yu, Z.Z.; Li, Y.L.; Pan, W.; Wang, H.Y.; Tang, B. Nuclear-targeted siRNA delivery for long-term gene silencing. *Chem. Sci.* **2017**, *8*, 2816–2822. [CrossRef] [PubMed]

254. Zhang, F.; Zhao, L.J.; Wang, S.M.; Yang, J.; Lu, G.H.; Luo, N.N.; Gao, X.Y.; Ma, G.H.; Xie, H.Y.; Wei, W. Construction of a Biomimetic Magnetosome and Its Application as a SiRNA Carrier for High-Performance Anticancer Therapy. *Adv. Funct. Mater.* **2018**, *28*, 1703326. [CrossRef]

255. Hematyar, M.; Soleimani, M.; Es-haghi, A.; Mokarram, A.R. Synergistic co-delivery of doxorubicin and melittin using functionalized magnetic nanoparticles for cancer treatment: Loading and in vitro release study by LC-MS/MS. *Artif. Cell Nanomed. B.* **2018**, *46*, S1226–S1235. [CrossRef] [PubMed]

256. He, Y.L.; Guo, S.W.; Wu, L.N.; Chen, P.W.; Wang, L.Y.; Ying, L.; Ju, H.X. Near-infrared boosted ROS responsive siRNA delivery and cancer therapy with sequentially peeled upconversion nano-onions. *Biomaterials* **2019**, *225*, 119501. [CrossRef]

257. Bian, Z.Y.; Yan, J.; Wang, S.M.; Li, Y.J.; Guo, Y.; Ma, B.H.; Guo, H.; Lei, Z.J.; Yin, C.; Zhou, Y.; et al. Awakening p53 in vivo by D-peptides-functionalized ultra-small nanoparticles: Overcoming biological barriers to D-peptide drug delivery. *Theranostics* **2018**, *8*, 5320–5335. [CrossRef] [PubMed]